International Journal of Nanomedicine Dovepress

Open Access Full Text Article ORIGINAL RESEARCH

Tadalafil Enhances the Therapeutic Efficacy of Mesenchymal Stem Cells-Derived Exosomes in Pulmonary Hypertension by Upregulating miR-29a-3p

Yi Liu[1,2], Changqing He[1], Quanhai Zhong[3], Xianbao Shi[4], Hongyan Li[1], Gaoge Fu[1], Lixuan Guo[1], Churong Zhao[1], Lei Tian[1], Xin Li[1], Xue Jiao[1], Lina Shan[1]

[1]Department of Respiratory Disease, The First Affiliated Hospital, Jinzhou Medical University, Jinzhou, 121000, People's Republic of China; [2]Department of Critical Care Medicine, Panzhihua Central Hospital, Panzhihua, 61700, People's Republic of China; [3]Clinical Drug Laboratory, People's Hospital of Yichun City, Yichun, Jiangxi, 336000, People's Republic of China; [4]Department of Pharmacy, The First Affiliated Hospital of Jinzhou Medical University, Jinzhou, People's Republic of China

Correspondence: Lina Shan, Email shanlina321@163.com

Introduction: Pulmonary hypertension (PH) is a progressive and life-threatening condition. Recent research has demonstrated that exosomes derived from mesenchymal stem cells (MSC) exhibit significant therapeutic potential in the treatment of PH. The composition of these exosomes is often substantially influenced by the characteristics of their parental cells. This study aimed to identify an intervention strategy to enhance the efficacy of mesenchymal stem cell exosomes in treating PH.

Methods: Exosomes were isolated from control MSC and tadalafil-pretreated MSCs. In vitro and in vivo studies were conducted.

Results: $MSC^{TAD\text{-}Exo}$ attenuated macrophage inflammation and improved endothelial cell (EC) apoptosis while also reducing pulmonary arterial pressure in a hypoxia-induced rat model. Furthermore, MSC exosomes can mitigate hypoxia-induced proliferation and migration of smooth muscle cells (SMC) by influencing the secretion of endothelial exosomes. MiR-29a-3p has been identified as a crucial mediator in this process, with its expression regulated by cAMP responsive element binding protein 1 (CREB1). MiR-29a-3p exerts anti-inflammatory effects by modulating the expression of ectonucleotide pyrophosphatase/phosphodiesterase 2 (ENPP2). Notably, the anti-inflammatory and anti-vascular remodeling activities of exosomes were diminished following the depletion of MiR-29a-3p.

Discussion: MSC treated with tadalafil can secrete better exosomes. $MSC^{TAD\text{-}Exo}$ may enhance anti-inflammatory and anti-vascular remodeling properties by upregulating mir-29a-3p expression, providing a novel idea for PH therapy. Future studies could explore the clinical application of this finding.

Keywords: exosome, tadalafil, hypoxia pulmonary hypertension, mesenchymal stem cell, miR-29a-3p

Introduction

Pulmonary hypertension (PH) is a clinical condition presenting as a progressive increase in pulmonary vascular resistance, and it eventually leads to right ventricular failure. PH remains incurable despite the progress made in treatment.[1] Histopathologically, PH involves intimal hyperplasia of small arteries exhibiting concentric or eccentric laminar sclerosis, medial hypertrophy, and adventitia hyperplasia with varying degrees of inflammatory reactions.[2] Despite recent advances in PH treatment, new tools must be urgently developed for the effective treatment of this disease.

Stem cell- and progenitor cell-based therapies have offered promising results in the treatment of several PH-associated lung diseases by transplanting different stem and progenitor cells, such as mesenchymal stem cells,[3,4] induced pluripotent stem cells,[5] and endothelial progenitor cells.[6] Experimental PH can be effectively prevented, treated, or reversed. Intravenously administered bone marrow MSCs improve core disease features, enhance vascular remodeling, and reduce right ventricular

Received: 25 August 2024
Accepted: 10 December 2024
Published: 19 December 2024

Graphical Abstract

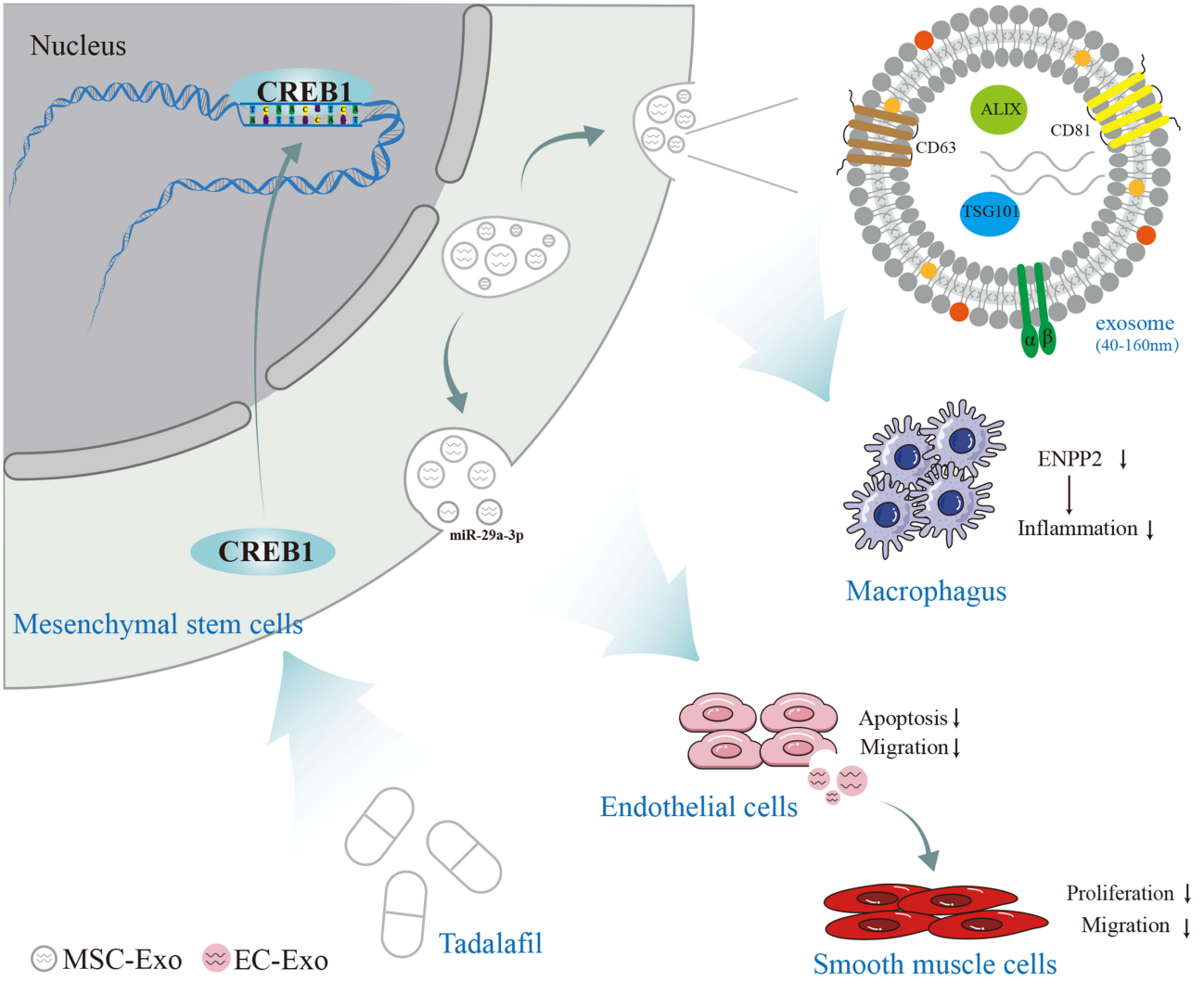

pressure in monocrotaline-induced and hypoxia-induced PH models.[7] MSCs seldom directly target the affected organs. This suggests that the immunomodulatory and therapeutic effects of MSCs may be paracrine.[8,9]

Current treatment modalities for pulmonary arterial hypertension, including endothelin receptor antagonists, phosphodiesterase-5 inhibitors, and prostacyclin analogs, have demonstrated varying degrees of efficacy; however, they often provide limited symptom relief and fail to prevent disease progression or improve vascular remodeling. In recent years, mesenchymal stem cell-derived exosomes have emerged as a promising therapeutic approach due to their ability to modulate inflammation, promote angiogenesis, and enhance tissue repair, fundamentally improving vascular remodeling. For example, MSC-derived exosomes can mitigate vascular remodeling by modulating NF-κB signaling or the Wnt5a/BMP signaling pathway.[10,11] Thus, they are considered a viable treatment option for PH. Exosomes are extracellular, membrane-bound vesicles of 30–150-nm diameters that transfer their bioactive molecules between cells.[12] The therapeutic properties of MSC-derived exosomes have been demonstrated in PH models.[13–15] However, the complex components of exosomes often vary dramatically depending on parent cell conditions, and thus exosomes perform different biological functions. Exosomes secreted by drug-treated or molecularly modified MSCs often exhibit more favorable therapeutic effects than those secreted by untreated MSCs in wide fields of application.[16–18] Tadalafil (TAD),

a long-acting PDE5 inhibitor, is commonly used clinically to treat PH, heart failure, and coronary artery disease. Tadalafil pretreatment of MSCs enhances their survival and proliferation by promoting cGMP/protein kinase G activity.[19,20] However, the effect of TAD on MSC-derived exosomes remains unclear. Given the potential benefits of using exosomes rather than stem cells alone for therapeutic purposes,[21,22] determining whether TAD pretreatment affects the secretion and function of exosomes from MSCs is more critical.

In this study, we explored the anti-inflammatory and anti-vascular remodeling effects of exosomes derived from TAD-pretreated MSCs (MSC^{TAD}-Exo) in vivo and in vitro and identified the underlying mechanisms. MSC^{TAD}-Exo significantly ameliorated lipopolysaccharide (LPS)-induced macrophage inflammation as well as hypoxia-induced migration and serum-free-induced apoptosis of endothelial cells (ECs) compared with exosomes derived from unpretreated MSCs.

Materials and Methods

A Model of Hypoxia-Induced PH

The 42 Sprague–Dawley (SD) male rats (age: 6–8 weeks) used in this study were healthy and donated by Jinzhou Medical University. Most animal studies have demonstrated that female sex and estrogen supplementation are factors that have a protective effect against PH. The animals were maintained under normal conditions with free access to food and water. The Jinzhou Medical University Research Ethics Committee approved all animal testing and procedures (2022031001). All our animal experiments were conducted in accordance with the guidelines of the National Animal Society. Sugen5416 (Su5416) is an exogenous compound inhibiting vascular endothelial growth factor receptor protein tyrosine kinase 1/2 (VEGFR1/2). Rats administered Su5416 in conjunction with chronic hypoxia (SuHx) develop a severe PH phenotype.[23] The rats were randomized into control, SuHx, and various exosome treatment groups. The control group rats spent 21 days under normoxia (21% O_2). The SuHx group rats were subcutaneously injected with Su5416 (Bio-Techne, Minneapolis, MN, USA), which was suspended in 0.5% [w/v] carboxymethylcellulose sodium, 0.9% [w/v] sodium chloride, 0.4% [v/v] polysorbate 80, 0.9% [v/v] benzyl alcohol in deionized water. Further, these rats were housed in a hypoxic chamber (10% O_2) for 3 weeks. The rats in the various exosome treatment groups were injected three times a week with 25 μg of relevant exosomes on the basis of the SuHx group (n = 6/group). The exosome protein concentration was determined using the bicinchoninic acid (BCA) kit (Beyotime, P0010). All workers who collected and analyzed the data (hemodynamics and histopathology measurements) were unaware of each animal's treatment status. No rats died before euthanasia.

Animal Experiments

Before the rats were sacrificed, they were intraperitoneally injected with sodium pentobarbital anesthesia (40 mg/kg). Next, a pre-filled heparin copper PE-50 catheter (Taimeng, Chengdu, China) was inserted into the appropriate site through the right external jugular vein. To measure the right ventricular systolic pressure (RVSP, mm Hg), the other end of the catheter was connected to a multiconductor physiological recorder with a pressure transducer (Taimeng, Chengdu, China). Pulmonary artery systolic pressure can be indirectly determined by recording RVSP. The right ventricle (RV) was dissected from the left ventricle (LV) and septum (S). These samples were weighed to determine the extent of RV hypertrophy (RVHI), which was expressed as the RV/(LV + S) ratio. For conducting the biochemical tests, the right lung was removed, snap-frozen in liquid nitrogen, and cooled to −80°C. The left lung was perfused with 4% paraformaldehyde, dehydrated in a gradient of 20% and 30% sucrose solution, and embedded with OCT. Hematoxylin and eosin (HE) were used to stain the sections. The percentages of medial wall thickness (WT%) and medial wall area (WA%) were calculated as follows: (WT/external diameter) × 100 = WT%; and WA% = (medial WA/total vessel area) × 100.

Measurement of Distance Traveled

To evaluate the exercise capacity of the rats, their maximal running distance on a motor-driven treadmill was measured. The belt speed was 10 m/min for the initial 5 min and was increased by 5 m/min every 5 min, with the maximum speed being 25 m/min for 15 min. After 30 min or when the rat ran out of energy, the test was terminated. The exercise was ceased when the rats exhibited fatigue. Fatigue was defined as the mouse or rat spending >5 consecutive seconds on the shock grid.

Cell Culture

Human pulmonary artery endothelial cells (HPAECs, Catalog #3100) and human pulmonary artery smooth muscle cells (HPASMCs, Catalog, #3110) were purchased from ScienCell. The cells were grown in endothelial cell culture medium (Cat. #1001) and smooth muscle cell medium (Cat. #1101), respectively. The HPAECs and HPASMCs were used in passages 3–8. The usual incubator settings for cell culture were 37°C, 21% O_2, and 5% CO_2. serum-free, hypoxia (1% O2) for 48 h, and exosome (2 μg/mL) treatments were applied to the cells.

The RAW264.7 cell line was generously donated by Professor Mingxin Liu of Jinzhou Medical University and procured from Procell Life Science & Technology Co., Ltd.[24] The cells were cultured in high-glucose Dulbecco's modified Eagle's medium (DMEM) (SH30022.01, HyClone, USA), supplemented with 10% fetal bovine serum (FBS) (10099141C, Gibco, USA). Subsequently, the cells were treated with lipopolysaccharide (LPS) at a concentration of 100 nM and exosomes at a concentration of 20 μM.

Male SD rats (60–80 g) were sedated with isoflurane through inhalation and sacrificed through cervical dislocation to isolate MSCs. Bone marrow cells from the femur and tibia were washed with a culture medium. The cells were seeded in culture dishes containing 10% FBS, Iscove's Modified Dulbecco's Medium (31980030, Gibco USA), and 100 mg/mL of streptomycin and 100 U/mL of penicillin. The cells were grown in a humidified atmosphere under 5% CO_2 at 37°C. To eliminate non-adherent cells, the medium was changed for the first time after a 24-h period. Every 3 days, a completely new medium was added to replace the old medium. The MSCs were subcultured 1:3 after they had reached approximately 80% confluence in each primary culture. MSCs at passages 3–4 were pretreated with 10 μmol/L TAD (Sigma, USA) in exosome-free IMDM for 48 h until the conditioned medium was collected.

Coculture System

For coculture experiments, HPAECs were inoculated in the transwell inserts. Once the cells reached 70–80% confluence, PBS, MSC-Exo, MSC^{TAD}-Exo, or GW4869 (Inhibitors of exosome synthesis/release. 20 μM) was added for 12 h. HPASMCs were then cultivated in 24-well plates. As soon as the cells reached 70–80% confluence, the controls or HUVECs were inserted into the HPASMC wells and exposed to hypoxia for 24 h (1% O2). Afterward, the cells were stained according to the EDU staining procedure, and the results were observed through fluorescence microscopy.

CCK8

Cell viability was determined using the CCK-8 test kit (K1076l; APExbio, USA). Briefly, MSCs were inoculated in a 96-well plate, and different concentrations of TAD were added to the plate. The plate was incubated for 24 h, and 10 μL of CCK-8 solution was added to each well. The plate was incubated for 1.5 h. Finally, an enzyme marker at 450 nm was used to measure the absorbance.

Western Blot Assay

MSCs and RAW264.7 were placed in the Radio Immunoprecipitation Assay buffer (P0013B, Beyotime, Beijing, China) for lysis. Protease inhibitors (ST506; Beyotime) and phosphorylase inhibitors (KGP602, KeyGEN, Jiangsu, China) were added, and all extracted proteins were quantified using the BCA protein quantification kit. The lysate samples were separated using sodium dodecyl sulfate-polyacrylamide gel electrophoresis and transferred to a PVDF membrane. Then, the membrane was incubated overnight at 4°C with primary antibodies, including rabbit anti-IL-6 (1:1000, sc-32296; Santa Cruz), rabbit anti-TNFα (1:1000, sc-12744; Santa Cruz), rabbit anti-IL-1β (1:1000, sc-12742; Santa Cruz), rabbit anti-ENPP2 (1:1000, ab140915, Abcam, USA), rabbit anti-CREB1 (1:1000, ab178322; Abcam, USA), rabbit anti-CCAAT/enhancer binding protein alpha (CEBPα) (1:10,000, EP709Y; Abcam), rabbit anti-Sp1 transcription factor (SP1) (1:1000, WL02251; Wanleibio, Shenyang, China), and immunoblot primary antibody diluted with 1% bovine serum albumin. After washing the membrane with PBS-Tween-20 (PBS-T), the membrane was incubated with the corresponding HRP-labeled secondary antibody (1:10,000, ab7090; Abcam) for 60 min. Finally, the membrane was covered with the ECL reagent (Beyotime, Shanghai, China). ImageJ software was used to measure the grayscale values, and each experiment was performed at least three times.

EDU Proliferation Assay

HPASMC and HPAEC proliferation was evaluated using the 5-ethynyl-2′-deoxyuridine (EDU) Cell Proliferation Assay Kit (K1076l; APExbio). The cells were seeded into 6-well plates (5×10^4 cells/well) and incubated under normoxic or hypoxic conditions. The cells were incubated for 2 h at 37°C after 1 mL of EDU (dilution reagent A to complete media at a 1:500 ratio) was added to each combination. In addition, the cells were fixed with 4% paraformaldehyde for 20 min and incubated for 30 min with 0.5 mL of the indicated click response solution per well.

Cell Migration Assay

To determine cell migration, transwell and cell scratching tests were conducted. Following different therapies, the cells (5×10^5 cells/well) were seeded into 6-well culture plates and allowed to grow until confluence. Next, a line was scraped through each cell by using a clean 200-μL pipette tip. Subsequently, the remaining cells were washed three times with PBS and allowed an extra day to grow in a serum-free medium. An inverted light microscope (IX71, Olympus Corporation, Japan) was used to measure the migration breadth. The images were captured by microscope (DM1000; Leica, Wetzlar, Germany) after 0 and 24 h. The transwell assays were conducted using 24-well plates. First, the top chamber was filled with 200 μL of FBS-free cell suspension (a total of 10,000 cells), and the bottom chamber was filled with 600 μL of FBS-containing media. At 24 h of treatment with different methods, the cells on the membrane's lower surface were stained with 1% crystal violet for 15 min after they were fixed with 4% paraformaldehyde. The unmigrated cells were removed from the upper surface of the membrane by using a cotton swab. Finally, the light microscope (DM1000; Leica, Wetzlar, Germany) was used to count the cells.

Cell Transfection

China's Genechem Co., Ltd. provided the small interfering RNAs (siRNAs) for cAMP-responsive element binding protein 1 (CREB1), CEBPα, and Enpp2. Supplementary Table 1 lists the knockdown sequences. Silencing RNA was used as a negative control. The cells (5 × 105 cells/well) were seeded into 6-well plates and transfected with the relevant siRNA (50 nmol/well) by using the Lipofectamine 2000 reagent (11668027, Invitrogen). To evaluate ENPP2 over-expression, the empty vector pcDNA3.1 was used as a control). The miR-29a-3p mimic (agomir) and miR-29a-3p inhibitor (antagomir) were obtained from GenePharma Co., Ltd (Shanghai, China).

Exosome Extraction and Characterization

MSCs were treated with TAD (10 μM) and cultivated in IMEM medium supplemented with 2% exosome-depleted serum (Gibco, A2720801, USA). The Umibio® exosome isolation kit (Umibio, UR52121, China) was used to separate exosomes from the cell supernatant. To remove the cells and debris, the culture medium was initially centrifuged at 3000 ×*g* at 4°C for 10 min and then at 10,000 ×*g* at 4°C for 20 min. The appropriate reagents were gradually added in proportion to the original sample volume. The mixtures were vortexed, incubated at 4°C for 1.5–2 h, and centrifuged at 10,000 ×*g* for 1 h at 4°C to precipitate exosome pellets. The pellets were resuspended in PBS. The exosomes were isolated and promptly stored at −80°C until they were used again. Using the ZetaView PMX 110 Particle Size Analyzer and Particle Counter (Particle Metrix Ltd)., the exosome size distribution and concentration in the liquid suspension were tracked and investigated. Western blotting was performed to verify the existence of exosome membrane markers. First, 8 μg of protein was added from the exosome samples into each well of 10% SDS/PAGE gels, and the gels were electrophoresed. Exosome biomarkers, such as anti-TSG101 (Abcam, ab125011, 1:2000), anti-CD63 (Abcam, ab134045, 1:1000), and anti-CD9 antibodies (Abcam, ab307085, 1:1000), were incubated with polyvinylidene fluoride (PVDF) membranes (Immobilon, IPVH00010). HRP-linked goat anti-rabbit IgG (1:10,000, ab7090; Abcam) was used as the secondary antibody. The enhanced chemiluminescence (ECL) reagent (Beyotime, P0018M) was used to visualize target bands by using a ChemiDoc™ Imager (Bio-Rad, USA). Image J software was employed to detect the relative intensity of the immunoreactive bands.

Immunofluorescence Assay

The lung sections were stained with immunofluorescence to identify intima-media thickening in the lung arteries of various groups. In summary, lung tissues in each group were dehydrated and fixed. The sections were then embedded in OCT,

subsequently fixed for 20 min with 4% paraformaldehyde, permeabilized for 20 min with 0.5% TritonX-100, and sealed with goat serum for 1 h. The sections were then coincubated with the primary antibody, α-SMA, overnight at 4°C and coupled with Alexa fluor 647 (A-21245; Invitrogen, USA). A secondary antibody was incubated with the sections for 2 h at room temperature, and cell nuclei were restained with DAPI. The samples were analyzed through fluorescence microscopy.

ELISA

Supernatants from the RAW264.7 cell medium were collected for the subsequent cytokine analysis. ELISA was performed using ELISA kits, including mouse TNF-α (88–7324-88; Invitrogen, USA), mouse IL-6 (88–7064-88; Invitrogen, USA), and mouse interleukin 1 beta (IL-1β) (BMS6002; Invitrogen, USA), in accordance with the manufacturer's instructions.

Chromatin Immunoprecipitation-qPCR

The chromatin immunoprecipitation (CHIP) assay was conducted using a commercial kit (Beyotime, Shanghai, China). An anti-CREB1 antibody was used to immunoprecipitate CREB1–chromatin complexes. Anti-IgG (Santa Cruz, USA) served as a negative control. Supplementary Table 1 lists the primers for amplification.

Flow Cytometry

Following EDTA-free trypsin digestion, the adherent PASMCs were centrifuged three times at 300 ×*g* for 5 min at 4°C and rinsed with pre-cooled PBS. The cells (1 × 106 cells/mL) were suspended in 400 μL Annexin V (BestBio; Guangzhou, China) binding buffer. After the cells were treated with 5 μL AnnexinV-PE and 8 μL 7-AAD to stain the nuclei, they were incubated for 15 min at 4°C in the dark. The stained samples were kept on ice until they were detected using a flow cytometer (BD Biosciences, San Jose, USA). FlowJo software was used to analyze the data.

Bioinformatics and Dual Luciferase Reporter Gene Experiments

For bioinformatics analysis, putative targets of miR-29a-3p were searched using TargetScan (http://targetscan.org/) and miRDB (http://www.mirdb.org/). ENPP2, which was predicted as a miR-612 target, was then assessed through the luciferase reporter assay. Then, 3′-UTR of enpp2 containing wild-type (WT) or mutant-type (MT) binding sites of miR-29a-3p were synthesized by Genechem Co., Ltd. and inserted into the pmirGLO vector (Promega). The resultant constructs were denoted as 3′-UTR-wt and 3′-UTR-mu, and the specific binding region mutated from UGGUGCU to UUGCAAG, correspondingly. Using Lipofectamine 3000, MSCs were cotransfected with reporter plasmids 3′-UTR-wt or 3′-UTR-mu, and miR-29a-3p agomir or NC (agomir). Using the Dual Luciferase® Reporter assay kit from Promega, Renilla and fluorescent luciferase activities were investigated. Renilla luciferase and Firefly luciferase activities were normalized. To find transcription factors that can bind at 2000-bp upstream of mir-29a-3p, promoter studies were conducted using the databases JPSPAR (https://jaspar.genereg.net/), promo (https://alggen.lsi.upc.es/cgi-bin/promo_v3/promo/promoinit.cgi?dirDB=TF_8.3), and animalTF (http://bioinfo.life.hust.edu.cn/AnimalTFDB#!/). CREB1 was assumed to be the upstream target, and the binding site was identified using a dual luciferase assay. Mir-29a-3p promoter regions containing different CREB1-binding sites were cloned into PGL3-basic reporter vectors (Promega). When cotransfecting MSCs with luciferase vectors and different CREB1 vectors, the PGL3 control vector was used as a control to cotransfect the cells. Mutant plasmids were constructed to detect the binding specificity. The CREB1-specific binding region was mutated from TCACGCAA to ATCTCGTC.

Exosome Label

Purified exosomes were labeled with the fluorescent dye PKH26 by using the Red Fluorescent Cell Linker Kit (Solarbio Science & Technology Co., Ltd., Beijing, China). The exosomes were washed in PBS and ultracentrifuged twice to remove the excess dye. To ascertain whether the exosomes can be efficiently taken up by HPAECs, HPASMCs, and RAW264.7 in vitro. The cells in the culture received 4 μg/mL of the pre-labeled exosomes. Following a 6-h incubation with exosomes, the cells were washed with PBS, fixed with 4% paraformaldehyde, and stained with either CD68 (97778;

CST, USA) or actin, aortic smooth muscle (α-SMA) antibodies (19245; CST, USA) at 4°C for 8 h and then with 4',6-diamidino-2-phenylindole (DAPI) at room temperature for 15 min. Through confocal imaging, the cell uptake of tagged exosomes was ascertained. In vivo, the exosomes were labeled with a green fluorescent dye, PKH67, as previously mentioned, and 25 μg of the exosomes were injected into the tail vein each time three times a week. After 3 weeks, the tissues were stained with CD31 antibody at 4°C for 8 h and DAPI at room temperature for 15 min, and fluorescence microscopy (DM1000; Leica, Wetzlar, Germany) was performed to detect the tissue uptake of exosomes.

RT-qPCR

RNA was isolated using the TRIzol reagent (Invitrogen, Life Technology, USA). To quantitate miRNA-29a-3p expression, reverse transcription was performed using a specific stem-loop real-time PCR miRNA kit (C10211-2; RiboBio, China). The RNA concentration and quality were measured using an ultraviolet spectrophotometer. According to the manufacturer's instructions (C10712-2; RiboBio, China), a 10-μL reverse transcription reaction sample addition system was prepared, followed by amplification and quantification using the SYBR-labeled dye method. The miR-29a-3p primers were synthesized by Sangon Biotech (Shanghai, China). The PCR conditions were as follows: holding stage 95°C for 5 min; and 95°C for 15s, 60°C for 30s, and 72°C 10s for the cycling stage with 40 cycles. Supplementary Table 1 presents the PCR primers. Using U6 snRNA as a reference gene, data were calculated through the comparative $2^{-\Delta\Delta}$Ct method.

Exosomal miRNA Sequencing

miRNA sequencing was performed in both MSC-Exo and MSC^{TAD}-Exo. Differentially expressed miRNAs were identified on the basis of fold change > 2 and $P < 0.05$ with a threshold established for up- and downregulated genes.

Statistical Analysis

Data were expressed as mean ± standard deviation. All samples were independent, including those measured over time among the experimental samples. Statistical analysis was performed using GraphPad Prism 9.0. Student's *t*-test was conducted for two-sample analyses, and normal distributions were presumed. One-way analysis of variance with Tukey's post hoc test was performed for analyzing more than two samples. Each experiment was run at least three times.

Detailed description of reagents, cell lines, and experimental procedures are available in the Supplementary material.

Results

Characterization and Differentiation Potential of MSCs

MSCs were extracted from the bone marrow of the SD rats. After 3–4 generations, MSCs were typically spindle-shaped and adhered to the culture dish. Most MSCs stained positively for CD90 (Supplementary Figure 1A). Oil red O and alizarin red staining demonstrated that MSCs could develop into osteoblasts and adipocytes (Supplementary Figure 1B and 1C).

Exosome Characterization and Exosome Internalization

CCK8 experiments were conducted to determine the most precise and ideal delivery concentration of TAD. The viability of MSCs was the highest at a TAD concentration of 10 μM compared with other concentrations (Supplementary Figure 2A), and TAD pretreatment did not significantly alter MSC morphology (Supplementary Figure 2B). Transmission electron microscopy (TEM) revealed that MSC^{TAD}-Exo was approximately 100 nm in size (Figure 1A). NTA was used to quantify the exosome size distribution (Figure 1B). MSC-Exo and MSC^{TAD}-Exo was similar in size, and the MSC^{TAD}-Exo concentration was significantly higher than the MSC-Exo concentration (Figure 1A and B). To further determine whether TAD pretreatment increased exosome secretion, immunofluorescence staining was performed for rab27a (an exosome-synthesizing protein) and CD63. The TAD-treated MSCs had higher eRab27a and CD63 expression (Supplementary Figure 2C and 2D). Western blotting unveiled that the expression of exosome-specific markers CD9, CD63, and TSG101 was positive (Figure 1C). Because perivascular inflammation and blood vessel thickening are primary pathologic alterations of PH, we observed exosome uptake by ECs, macrophages, and SMCs. PKH26, a red fluorescent cell membrane dye, was used to pre-mark exosomes before they were added for uptake by growing recipient cells. After exosomes were added for 6 h, confocal images

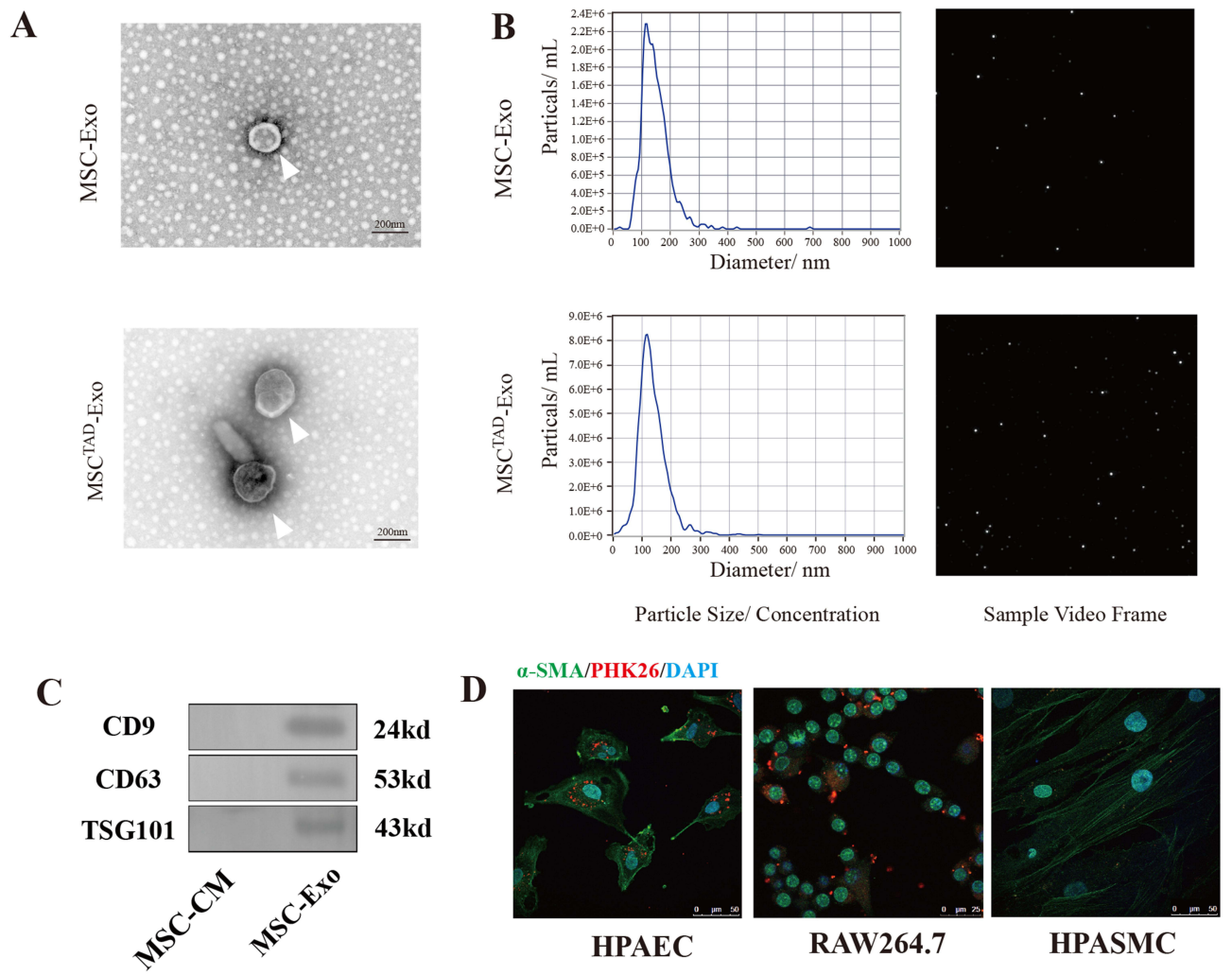

Figure 1 Characterization and functional validation of exosomes derived from TAD-treated MSCs. (**A**) Cup-shaped morphology of purified MSC-Exo and MSC^{TAD}-Exo (arrowhead) assessed by TEM. (**B**) The particle size, particle concentration, and video frame of MSC-Exo and MSC^{TAD}-Exo were analyzed by nanoparticle tracking analysis. (**C**) Representative images of Western blotting displaying the exosomal protein markers. (**D**) Representative confocal images show that red fluorescence dye PKH26-labeled exosomes were endocytosed by HPAECs, RAW264.7, and HPASMCs after a 6 h incubation. Scale bar = 50 μm. (**A**–**D**) n = 3.

revealed significant exosome uptake by the HPAECs and RAW264.7 cells. By contrast, the HPASMCs exhibited less exosome uptake (Figure 1D). These data show that ECs and inflammatory cells take up MSC-Exo more efficiently than SMCs.

TAD-Pretreated MSCs Attenuate Macrophage Inflammation and Inhibit EC Migration and Apoptosis

MSC-Exo attenuates LPS-induced inflammation in macrophages.[25,26] In this study, ELISA and Western blotting assays confirmed the same result that MSC-Exo decreased LPS-induced inflammation. Furthermore, MSC^{TAD}-Exo drastically reduced LPS-induced inflammation compared with MSC-Exo (Figure 2A–C and Supplementary Figure 3A). EC injury during PH development is considered an initiator of vascular remodeling. We further explored the effect of exosomes on EC injury. To assess the optimal dosage of exosomes, different concentrations of MSC^{TAD}-Exo were added to the HPAECs, and their ability to inhibit hypoxia-induced EC migration was evaluated. When the HPAECs were treated with 0–2 μg/mL MSC^{TAD}-Exo, migration reduced dose-dependently. However, when 2–4 μg/mL MSC^{TAD}-Exo was used, no statistical significance was detected (Supplementary Figure 3B). Thus, a dose of 2 μg/mL was selected for the in vitro assay. Compared with the hypoxic group, MSC-Exo markedly decreased cell migration. However, cell migration was more strongly inhibited by MSC^{TAD}-Exo than by MSC-Exo (Figure 2D and Supplementary Figure 3C). Similarly, MSC-

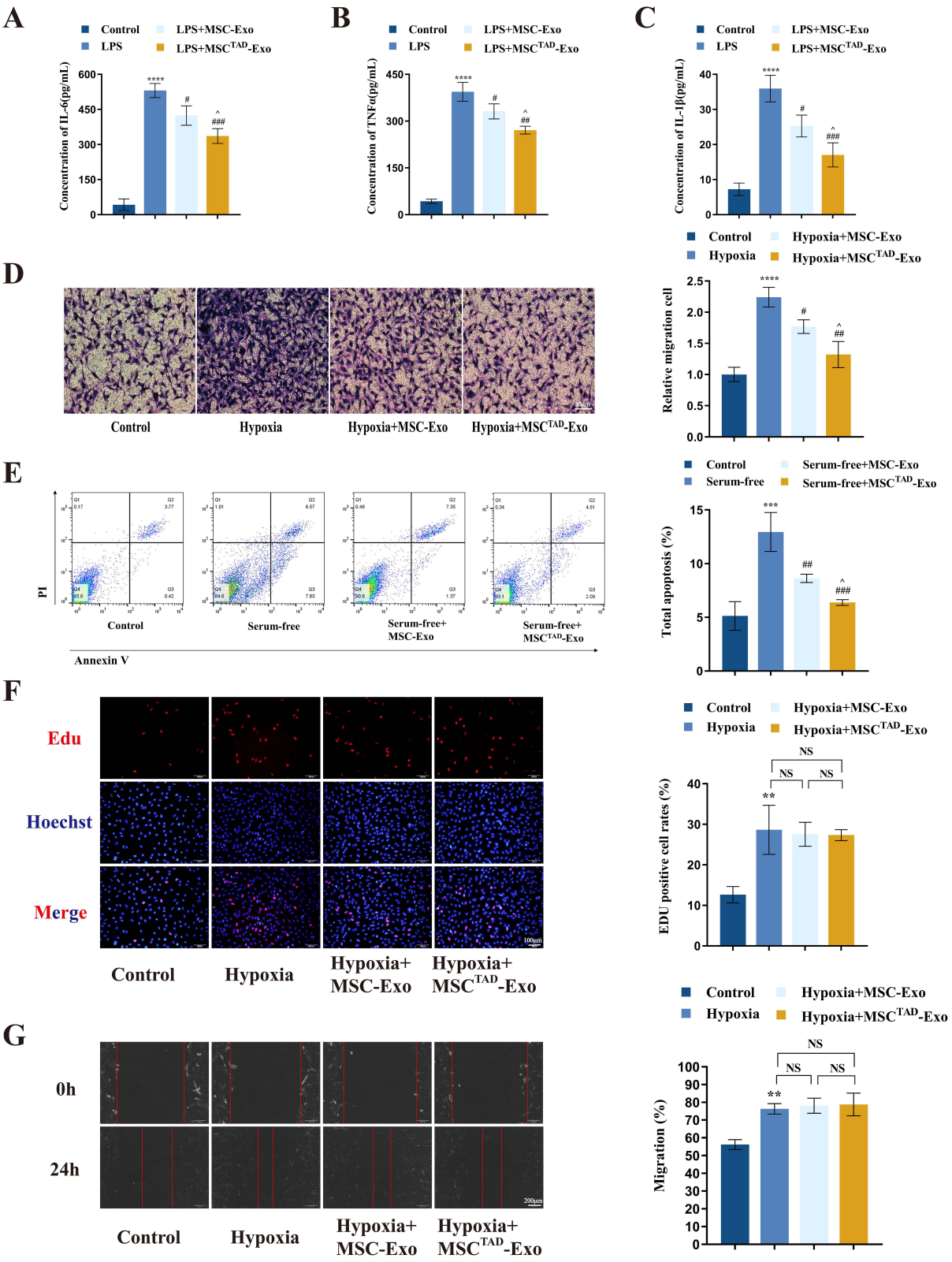

Figure 2 Effect of MSC^{TAD}-Exo on different cellular phenotypes (**A**–**C**) ELISA for the expression of pro-inflammatory factors IL-6, TNFα, and IL-1β (n = 3). ****P < 0.0001 vs Control; $^{\#}P$ < 0.05, $^{\#\#}P$ < 0.01, $^{\#\#\#}P$ < 0.001 vs LPS group; ^P < 0.05 vs MSC-Exo group; (**D**) Cell migration was assessed using Transwell assay. Scale bar, 50 μm (n = 5). ****P < 0.0001 vs Control; $^{\#}P$ < 0.05, $^{\#\#}P$ < 0.01, vs LPS group; ^P < 0.05 vs MSC-Exo group; (**E**) Scatter diagram of apoptosis in HPAECs treated with exosomes and negative control (n = 3). ****P < 0.0001 vs Control; $^{\#\#}P$ < 0.01, $^{\#\#\#}P$ < 0.001, vs Serum-free group; ^P < 0.05 vs Serum-free+ Serum-free+ MSC-Exo group; (**F**) Cell proliferation was assessed using Edu experiments (n = 5). Scale bar = 100 μm. **P < 0.01 vs Control; (**G**) Scratch experiment to detect cell migration. Cell migration was taken for comparison 0 and 24 h after scratching (n = 3). Scale bar = 200 μm. **P < 0.01 vs Control.

Exo and MSC^{TAD}-Exo efficiently protected the HPAECs from serum-free medium-induced apoptosis. Apoptosis levels significantly decreased in the MSC^{TAD}-Exo group compared with the MSC-Exo group (Figure 2E and Supplementary Figure 3D). These data suggest that MSC^{TAD}-Exo is more protective for ECs than MSC-Exo under the in vitro conditions we tested.

Exosomes Derived from MSCs Do Not Considerably Improve the Hypoxia-Induced Malignant Phenotype of SMCs

SMC migration and proliferation resulted in the luminal narrowing of pulmonary arteries and elevated pulmonary arterial pressure. MSC-Exo and MSC^{TAD}-Exo were added to the HPASMCs, and their effect on cell migration and proliferation were determined. Neither MSC-Exo nor MSC^{TAD}-Exo significantly prevented the emergence of a hypoxia-induced malignant phenotype of SMCs, which is consistent with our finding that MSC-Exo and MSC^{TAD}-Exo were less absorbed by SMCs (Figure 2F and G).

MSC^{TAD}-Exo Effectively Improves Vascular Remodeling and the Right Ventricular Function in a Rat Model of PH

To evaluate the potential benefits of exosomes in vivo, the rats were injected with MSC-Exo, MSC^{TAD}-Exo, and PBS three times a week through the tail vein. Four weeks later, the rat lungs were separated to determine the distribution of PKH67-labeled MSC-Exo and MSC^{TAD}-Exo. Exosomes were mainly distributed in the endothelium of the vasculature (Supplementary Figure 4A). Patients with PH frequently die from right ventricular failure. However, MSC-Exo and MSC^{TAD}-Exo were found to effectively reduce right ventricular hypertrophy in the SuHx rats (Figure 3B and Supplementary Figure 4B). In addition to morphology, we further detected the right ventricular function by using a treadmill. The motor function was significantly decreased in the SuHx rats and was slightly restored after MSC-Exo administration. The motor function significantly improved in the MSC^{TAD}-Exo group compared with the SuHx group (Supplementary Figure 4C). Moreover, MSC-Exo treatment could effectively reduce pulmonary arterial pressure. However, the decrease in pulmonary arterial pressure after MSC^{TAD}-Exo treatment was more significant than that after MSC-Exo treatment (Figure 3C). As for the remodeling of pulmonary vessels, HE staining revealed that vessel wall thickening was obvious in the SuHx group, and both MSC-Exo and MSC^{TAD}-Exo were effective in improving vascular remodeling. However, no statistically significant difference was observed between the two groups (Figure 3A–E and Table 1). Further, immunofluorescence staining of α-SMA was performed to observe the alteration of vascular media. Vascular media thickening was obvious in the SuHx group, whereas both MSC-Exo and MSC^{TAD}-Exo significantly attenuated vascular media thickening (Figure 3F). Considering that the HPASMCs were not involved in the uptake of exosomes, we hypothesized that MSC-Exo alleviates hypoxia-induced vascular media thickening in rats by regulating ECs.

MSC^{TAD}-Exo Attenuates the Promotion of SMC Proliferation and Migration by EC-Exo

We first examined the efficiency of HPASMCs to uptake EC-Exo (10μM).[27] The HPASMCs could efficiently take up PKH26-labeled EC-Exo within 6 h (Figure 4A). The HPAECs were incubated with PBS, MSC-Exo, and MSC^{TAD}-Exo for 18 h and further cultured in 10% exosome-free FBS medium for 48 h. The conditioned medium was collected to isolate the exosomes of each group. These exosomes secreted by pre-treated HPAECs were named as EC-Exo, EC$^{MSC\text{-}Exo}$-Exo, and EC$^{MSC(TAD)\text{-}Exo}$-Exo, respectively. Then, the HPASMCs were treated with EC-Exo, EC$^{MSC\text{-}Exo}$-Exo, and EC$^{MSC(TAD)\text{-}Exo}$-Exo, and the proliferation and migration of these cells were observed under hypoxia (Figure 4B). The EDU results revealed that EC-Exo significantly promoted the proliferation of hypoxia-induced HPASMCs, whereas the EC^{MSC}-Exo and EC^{MSCTAD}-Exo had a comparatively weaker promoting effect the proliferation (Figure 4C). The same result was observed in the scratch experiment, where EC-Exo significantly promoted the migration of hypoxia-induced HPASMCs, whereas EC^{MSC}-Exo and EC^{MSCTAD}-Exo weakly affected the migration (Figure 4D). These results suggest

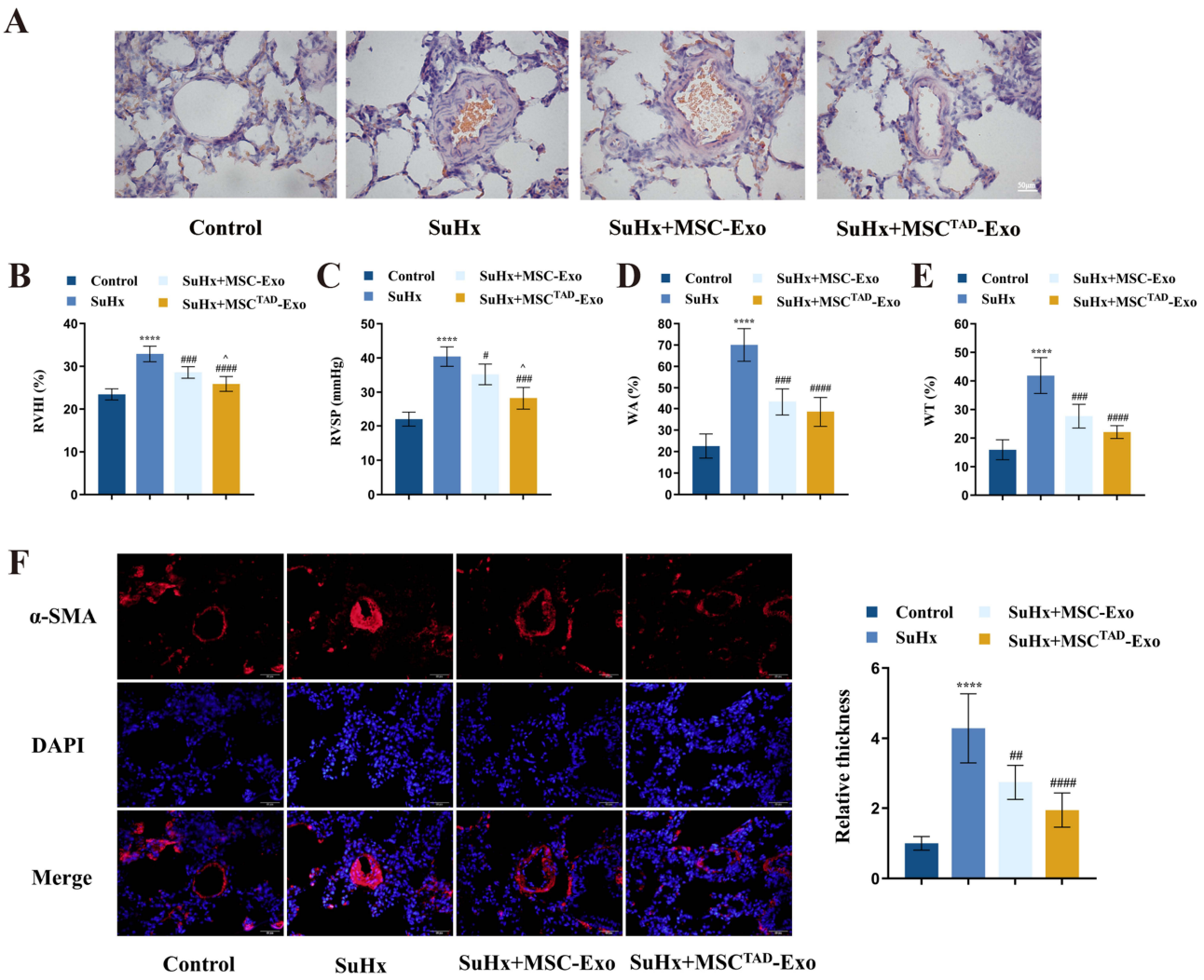

Figure 3 Effect of MSC^{TAD}-Exo on a model of hypoxia-induced pulmonary hypertension. (**A**) Representative image of HE staining performed to quantify the medial wall thickness of distal vessels. Scale bar = 50 μm. (**B**) Calculated as the weight ratio of RV and LV + S (RV/LV + (S). (**C**) RVSP was measured by right-sided heart catheterization with a pressure transducer microcatheter. (**D**) Proportion of the medial wall area. (**E**) The proportion of the medial wall thickness. (**F**) Thickening of the intima-media of small pulmonary vessels by immunofluorescence. Scale bar = 50 μm. (**A-F**) n = 6. ****$P < 0.0001$ vs Control; $^{\#}P < 0.05$, $^{\#\#}P < 0.01$, $^{\#\#\#}P < 0.001$, $^{\#\#\#\#}P < 0.0001$vs. SuHx group; ^$P < 0.05$ vs SuHx+ MSC-Exo group.

that MSC^{TAD}-Exo pretreatment significantly attenuated the malignant phenotype-promoting effect of HPAECs on HPASMCs.

Moreover, we conducted coculture experiments to confirm the protective effect of MSC^{TAD}-Exo on HPASMCs by affecting exosome secretion from HPAECs. We co-cultured HPASMCs and HPAECs and tested their interaction in the

Table 1 Hemodynamic and Morphologic Data

	Control	SuHx	SuHx + MSC-Exo	SuHx+ MSC^{TAD}-Exo
RVSP (mmHg)	22.0±2.1	40.4±2.9***	35.2±3.0$^{\#\#\#\#}$	28.1±3.3$^{\#\#\#\#\#\wedge}$
RVHI (%)	23.5±1.2	32.9±1.7****	28.6±1.2$^{\#}$	25.9±1.6$^{\#\#\#\wedge}$
WA (%)	22.6±5.6	70.1±7.6****	43.3±6.2$^{\#\#\#\#}$	38.6±6.8$^{\#\#\#\#\#}$
WT (%)	15.9±3.5	41.9±6.3****	26.5±3.1$^{\#\#\#\#}$	22.1±2.3$^{\#\#\#\#\#}$
Treadmill Distance (m)	467.5±71.5	210.0±49.1****	285.8±74.9	320.8±45.2$^{\#}$

Notes: ***$P < 0.001$, ****$P < 0.0001$ vs Control; $^{\#}P < 0.05$, $^{\#\#}P < 0.01$, $^{\#\#\#\#}P < 0.001$, $^{\#\#\#\#\#}P < 0.0001$vs. SuHx group; ^$P < 0.05$ vs SuHx+ MSC-Exo group.

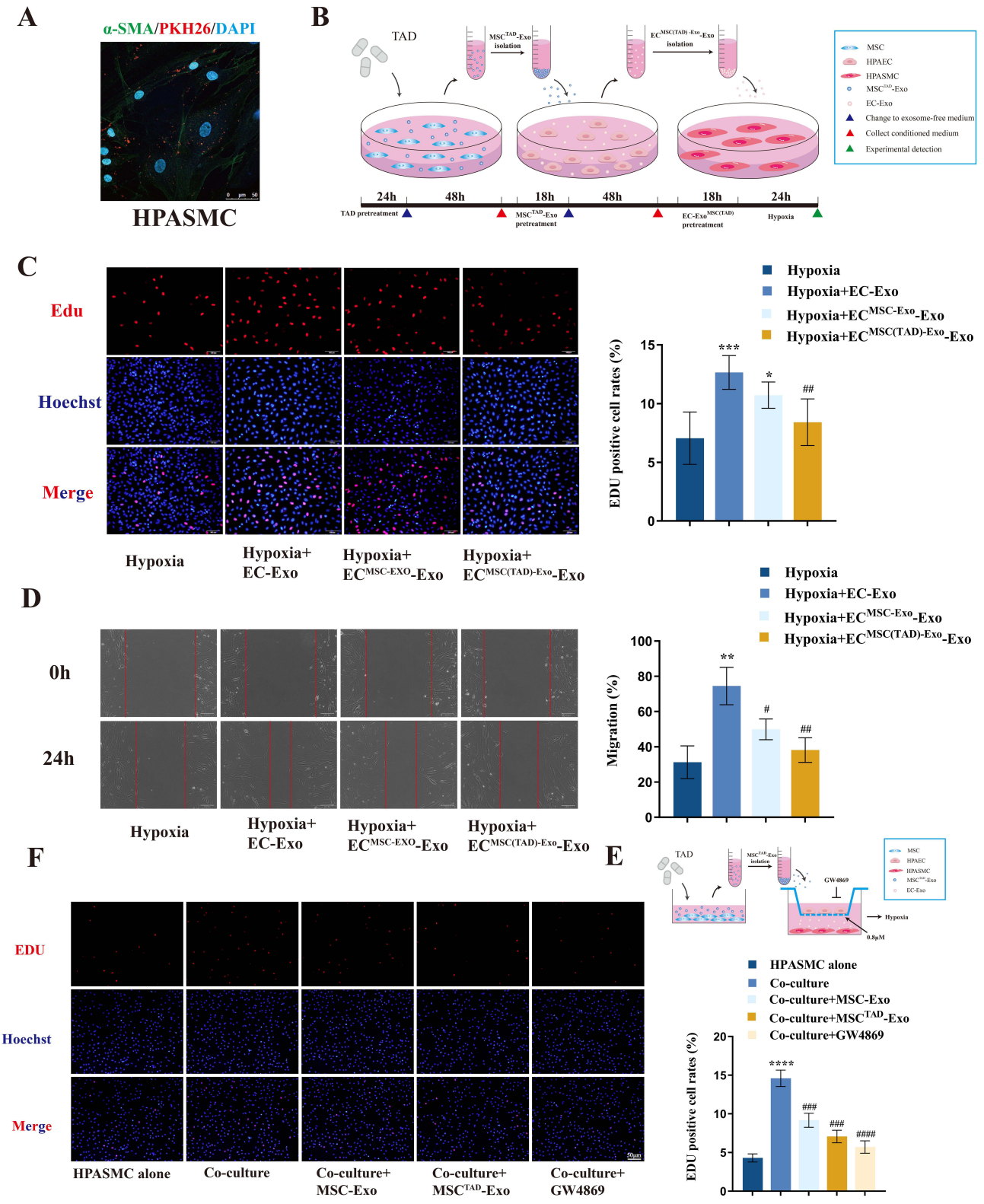

Figure 4 MSC^{TAD}-Exo pretreatment significantly attenuated the malignant promoting effect of HPAECs on HPASMCs. (**A**) Representative immunofluorescent images depicting that the red fluorescence dye PKH26-labeled HPAEC-derived exosomes were endocytosed by HPASMCs after 6 h of incubation. Scale bar = 50 μm. (**B**) Schematic of the EC-Exo-mediated HPASMC cells experiment. (**C**) Cell proliferation was assessed by Edu experiments (n = 5). Scale bar = 50 μm. *P < 0.05, ***P < 0.001, vs Hypoxia; $^{\#\#}P$ < 0.01, vs Hypoxia+ EC-Exo. (**D**) Migration of HPASMCs was measured 24 h after scratching, and HPASMCs were maintained in an FBS-free medium supplemented with exosomes (n = 3). Scale bar = 200 μm. **P < 0.01, vs Hypoxia; $^{\#}P$ < 0.05, $^{\#\#}P$ < 0.01, vs Hypoxia+ EC-Exo. (**E**) Schematic representation of the co-culture HPAECs with HPASMCs experiment by using the Transwell system (**F**) EDU assay for proliferation of HPASMCs after co-cultured with GW4869, MSC-Exo or MSC^{TAD}-Exo-pretreated HPAECs (n = 3). Scale bar = 100 μm. ****P < 0.0001 vs HPASMC alone; $^{\#\#\#}P$ < 0.001, $^{\#\#\#\#}P$ < 0.0001 vs Co-culture.

presence of MSC-Exo, MSC^{TAD}-Exo, and the exosome inhibitor GW4869 (Figure 4E). Compared with HPASMCs alone, the proliferation of HPASMCs co-cultured with HPAECs was significantly enhanced. By contrast, this proliferation-promoting effect was significantly attenuated with the addition of MSC-Exo or MSC^{TAD}-Exo or GW4869 (Figure 4F). In conclusion, our data suggest that ECs can take up MSC-Exo exosomes and secrete exosomes, thereby attenuating the malignant phenotype-promoting effect of ECs on HPASMCs under hypoxia.

TAD Pretreatment Increases miR-29a-3p Expression via CREB1

Increasing evidence has suggested that miRNAs in exosomes play a key role in cellular interactions.[28,29] To investigate the mechanisms underlying the protective effects of MSC^{TAD}-Exo on PH, we performed miRNA sequencing of MSC-Exo and MSC^{TAD}-Exo using Illumina instruments to identify differentially expressed miRNAs (Supplementary Table 2). In total, 6 miRNAs were identified to be upregulated (over 2-fold change) with MSC^{TAD}-Exo compared with MSC-Exo (Figure 5A and Supplementary Figure 5A). Among these upregulated miRNAs, miR-128p, miR-487b-3p, mir-139-5p, and miR-106-5p have not been reported to be involved in pulmonary arterial hypertension. MiR-210-3p can promote the formation of pulmonary arterial hypertension,[30] whereas miR-29a-3p exerted a protective effect against pulmonary arterial hypertension.[31,32] Thus, we hypothesized that miR-29a-3p was the key functional molecule of MSC^{TAD}-Exo. To test our hypothesis, miR-29a-3p expression in MSC and MSC-Exo was examined after TAD addition. The TAD pretreatment caused approximately 2-fold and 3-fold increases in miR-29a-3p expression in MSC-Exo and MSC^{TAD}-Exo, respectively (Figure 6A and B). To reveal the mechanism through which the TAD pretreatment increased miR-29a-3p expression, we first analyzed the potential promoter region of miR-29a-3p that can be bound by the transcription factor (2-kb upstream of the transcription start site) using JASPAR, Promo, and AnimalTF databases. This analysis resulted in three candidate molecules (SP1, CEBPα, and CREB1) after de-intersection (Figure 5B). After the addition of TAD, the protein expression of the three transcription factors in the MSCs was determined. TAD had no significant effect on SP1 expression, whereas it greatly upregulated CREB1 and CEBPα protein expression (Figure 5C). After CREB1 and CEBPα were knocked down in MSCs (Supplementary Figure 5B), TAD was added into MSC media, and sh-NC was used as a control. Compared with sh-NC, CREB1 knockdown significantly blocked the effect of TAD on miR-29a-3p and decreased its expression. However, CEBPα knockdown did not affect miR-29a-3p expression (Figure 5D). Further, CREB1 was knocked down to observe its effect on miR-29a-3p. CREB1 knockdown significantly decreased miR-29a-3p expression compared with sh-NC (Figure 5E). On cloning three miR-9a-3p promoter regions into a luciferase reporter system (LUC1-LUC3), we found that Luc3 luciferase activity was significantly decreased with the addition of overexpressed CREB1 compared with Luc1 and Luc2 luciferase activities (Figure 5F). This suggested that the CREB1 binding site within the miR-29a-3p promoter was between −750 and −1323 bp.

We further performed a CHIP assay and found that CREB1 was recruited to the −750- and −1323-bp regions (Figure 5J). Additionally, a putative CREB1 binding motif sequence was predicted in this region by using the promoter analysis tool JASPAR (Figure 5G and H). We subsequently constructed luciferase reporter plasmids with wild-type and mutant miR-29a-3p promoter sequences, named miR-29a-3p-wt and miR-29a-3p-mu, respectively. When the cells were transfected with miR-29a-3p-wt, CREB1 overexpression increased luciferase activity. Conversely, CREB1 overexpression cannot change the luciferase activity after miR-29a-3p-mu transfection (Figure 5I). These results collectively demonstrated that the miR-29a-3p promoter region at −832 to −839 bp is an effective binding site for CREB1.

miR-29a-3p Inhibits Inflammation Through ENPP2

We hypothesized that miR-29a-3p plays a mediator role in MSC^{TAD}-Exo. To test our hypothesis, miR-29a-3p was silenced in TAD-pretreated MSCs and overexpressed in untreated MSCs (Figure 6A). Then, the exosomes (MSC-Exo, MSC^{TAD}-Exo, $MSC^{TAD(antagomir)}$-Exo, and $MSC^{(agomir)}$-Exo) in these MSCs were extracted (Figure 6B). No significant morphological changes were observed in the knockdown versus overexpressed cells. As exosomes significantly ameliorated the LPS-induced inflammatory response, miR-29a-3p expression was examined in the RAW264.7 cells. The LPS+MSC^{TAD}-Exo group exhibited an approximately 3-fold increase in miR-29a-3p expression compared with the LPS+MSC-Exo group. LPS+MSC^{TAD}-Exo upregulated miR-29a-3p expression by approximately 5-fold compared with LPS, and the miR-29a-3p expression level in the LPS+$MSC^{(agomir)}$-Exo group was similar to that in the LPS+MSC^{TAD}-Exo group (Figure 6C). Treatment of RAW264.7 cells

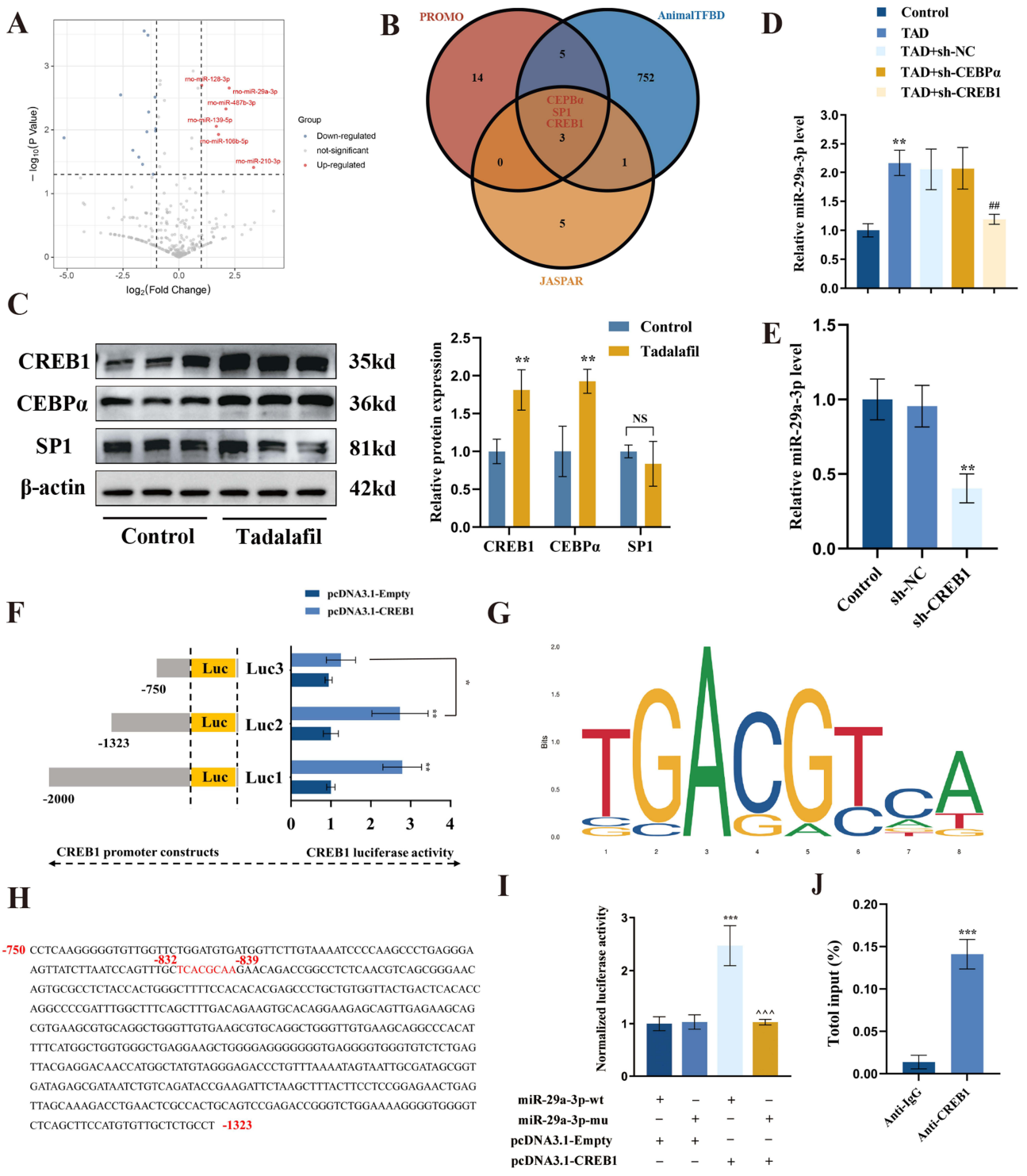

Figure 5 CREB1 binding to the promoter region regulates the miR-29a-3p expression. (**A**) Volcano plot showing log2 (Fold change) (MSC^{TAD}-Exo vs MSC-Exo) on the X-axis and -log10 (P value) on the Y-axis. MiR-29a-3p indicated in red was significantly increased in MSC^{TAD}-Exo after correction for multiple comparisons. (**B**) Venn diagram showing predicted proteins after the intersection of three databases. (**C**) Representative Western blot protein bands of SP1, CREB1, and CEBPα in MSCs (n = 3). $^{**}P < 0.01$ vs Control; (**D**) The MiR-29a-3p expression after tadalafil treatment while knocking down different proteins (n = 3). $^{**}P < 0.01$ vs Control; $^{\#\#}P < 0.01$ vs TAD; (**E**) Expression of miR-29a-3p after knockdown of CREB1 (n=3). $^{**}P < 0.01$ vs sh-NC; (**F**) Luciferase activities of different miR-29a-3p promoter reporter constructs, co-transfected with CREB1 or a negative control (n = 3). $^{**}P < 0.01$ vs pcDNA3.1-Empty; (**G**) DNA recognition sequence of CREB1; (**H**) One putative CREB1-binding sites in the miR-29a-3p promoter. (**I**) Relative luciferase activity (Firefly/Renilla) of vectors containing the wild-type CREB1-binding sites (miR-29a-3p-wt) or mutant-binding sites (miR-29a-3p-mu) of miR-29a-3p promoter in MSCs transduced with CREB1-expressing vector (pcDNA3.1-CREB1) or control vector (pcDNA3.1) (n = 3). $^{***}P < 0.001$ vs miR-20a-3p-mu+pcDNA-Empty; $^{\wedge\wedge\wedge}P < 0.001$ vs miR-20a-3p-wt+pcDNA-CREB1. (**J**) CHIP-qPCR analysis in the region (−750) ~ (−1323) of the miR-29a-3p promoter (n = 3). $^{***}P < 0.001$ vs Anti-IgG.

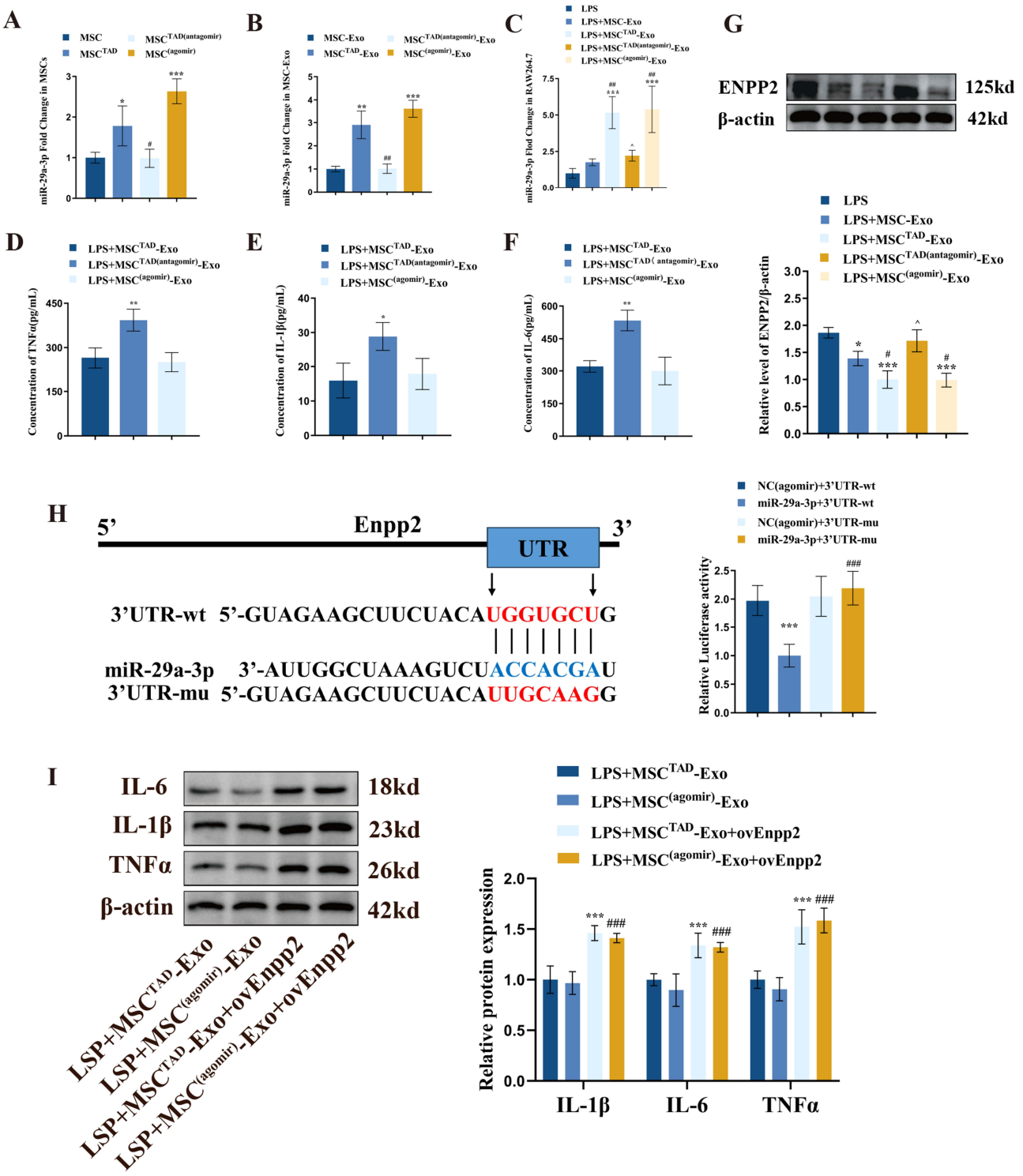

Figure 6 MiR-29a-3p regulates inflammation through ENPP2; (**A**) The expression values for miR-29a-3p in MSCs treated by PBS, TAD, TAD (antagomir), or agomir tested by RT-qPCR. *P < 0.05, ***P < 0.001 vs MSC; $^{\#}P$ < 0.05 vs MSC^{TAD}; (**B**) The expression values for miR-29a-3p in MSC-Exo treated by PBS, TAD, TAD(antagomir), or agomir tested by RT-qPCR. **P < 0.01, ***P < 0.001 vs MSC-Exo; $^{\#\#}P$ < 0.01 vs MSC^{TAD}-Exo; (**C**) The expression values for miR-29a-3p in RAW264.7 treated by different MSC-Exo. ***P < 0.001 vs LPS; $^{\#\#}P$ < 0.01 vs LPS+MSC-Exo; $^{\wedge}P$ < 0.05 vs LPS+MSC^{TAD}-Exo; (**D–F**) ELISA for the expression of pro-inflammatory factors IL-6, TNFα, and IL-1β. *P < 0.05, **P < 0.01 vs LPS+MSC^{TAD}-Exo; (**G**) The protein expression of ENPP2 after treatment with different groups of exosomes. *P < 0.05, ***P < 0.001 vs LPS; $^{\#}P$ < 0.05 vs LPS+MSC-Exo; $^{\wedge}P$ < 0.05 vs LPS+MSC^{TAD}-Exo; (**H**) One region in the enpp2 3'-UTR was predicted to bind with miR-29a-3p. ***P < 0.001 vs.NC (agomir)+ 3'-UTR-wt; $^{\#\#\#}P$ < 0.001 vs miR-29a-3p+3'-UTR-wt; (**I**) Proinflammatory factor protein expression in different treatments. (**A–I**) n = 3. ***P < 0.001 vs LPS+ MSC^{TAD}-Exo; $^{\#\#\#}P$ < 0.001 vs LPS+MSC$^{(agomir)}$-Exo.

with LPS+ $MSC^{TAD(antagomir)}$-Exo significantly attenuated the anti-inflammatory effect of LPS+ MSC^{TAD}-Exo, whereas LPS +$MSC^{(agomir)}$-Exo exerted an effect similar to that of LPS+MSC^{TAD}-Exo (Figure 6D–F and Supplementary Figure 5C). The downstream target genes of miR-29a-3p were analyzed using TargetScan in conjunction with miRBD. ENPP2 was found to be a candidate target gene of miR-29a-3p. ENPP2 is a mature protein having lysophospholipase D activity and is significantly overexpressed in various inflammatory responses.[33,34] In our study, ENPP2 protein expression was significantly negatively correlated with miR-29a-3p (Figure 6C and G). We overexpressed or knocked down miR-29a-3p in MSCs, separated exosomes from MSCs, added them into the Raw264.7 cells, and detected the ENPP2 protein level in these cells. Compared with the LPS +MSC-Exo group, ENPP2 expression levels in both LPS+MSC^{TAD}-Exo and LPS+$MSC^{(agomir)}$-Exo groups significantly decreased. Subsequently, the dual luciferase reporter gene assay unveiled that miR-29a-3p-wt could bind to ENPP2 3′UTR, whereas miR-29a-3p-mu could not (Figure 6H). To further validate that ENPP2 is a key protein that allows miR-29a-3p to exert its anti-inflammatory function, an ENPP2 overexpression vector was constructed (Supplementary Figure 5D). According to Western blotting, the anti-inflammatory effects of MSC^{TAD}-Exo and $MSC^{(agomir)}$-Exo were attenuated after ENPP2 over-expression (Figure 6I). Therefore, our data suggest that miR-29a-3p exerts its potent anti-inflammatory effect by inhibiting ENPP2 expression.

miR-29a-3p Mediates the Inhibitory Effect of MSC^{TAD}-Exo on EC Migration and Apoptosis

As exosomes were internalized by ECs, we determined miR-29a-3p expression in HPAECs under different treatment conditions. MSC^{TAD}-Exo or $MSC^{(agomir)}$-Exo treatment increased miR-29a-3p expression in the HPAECs (Figure 7A). The transwell results revealed that the $MSC^{TAD(antagomir)}$-Exo group exhibited a significant increase in EC migration compared with the MSC^{TAD}-Exo group, whereas the $MSC^{(agomir)}$-Exo and MSC^{TAD}-Exo groups exerted a similar inhibitory effect on EC migration (Figure 7B). The scratch experiments also supported the same conclusion (Supplementary Figure 6A). The flow cytometry results demonstrated that miR-29a-3p knockdown significantly reduced the inhibitory effect of MSC^{TAD}-Exo on cell apoptosis, whereas miR-29a-3p overexpression exhibited the same therapeutic effect as TAD pretreatment (Figure 7C) and the same results were obtained through Hoechst staining (Supplementary Figure 6B).

miR-29a-3p in MSC^{TAD}-Exo Weakens the Interaction Between ECs and SMCs

Because the protective effect of MSC^{TAD}-Exo on SMCs is exerted by attenuating malignant EC-Exo (Figure 4), we tested miR-29a-3p expression in exosomes secreted by HPAECs after different treatments. Interestingly, higher miR-29a-3p levels were still detected in $EC^{MSCTAD\text{-}Exo}$-Exo and $EC^{MSC(agomir)\text{-}Exo}$-Exo compared with EC-Exo (Figure 7D). The EDU experiments unveiled that $EC^{MSCTAD(antagomir)\text{-}Exo}$-Exo resulted in enhanced cell proliferation compared with $EC^{MSCTAD\text{-}Exo}$-Exo, whereas $EC^{MSC(agomir)\text{-}Exo}$-Exo had the same protective effect as $EC^{MSCTAD\text{-}Exo}$-Exo (Figure 7E). The transwell assay revealed that $EC^{MSCTAD(antagomir)\text{-}Exo}$-Exo resulted in enhanced cell migration compared with $EC^{MSCTAD\text{-}Exo}$-Exo, and miR-29a-3p overexpression exhibited the same protective effect as $EC^{MSCTAD\text{-}Exo}$-Exo (Figure 7F).

miR-29a-3p Mediates the Protective Effects of MSC^{TAD}-Exo on Vascular Remodeling and Ventricular Function

To investigate whether miR-29a-3p mediates the beneficial effects of MSC^{TAD}-Exo on cardiac and vascular functions, MSC^{TAD}-Exo, $MSC^{TAD(antagomir)}$-Exo, and $MSC^{(agomir)}$-Exo were delivered into rats. Then, changes in pulmonary vascular remodeling and right ventricular pressure were observed after 4 weeks of SuHx treatment. Regarding cardiac function measurements, $MSC^{TAD(antagomir)}$-Exo increased the right ventricular weight, decreased exercise distance, and increased pulmonary arterial pressure compared with MSC^{TAD}-EXO. Interestingly, $MSC^{(agomir)}$-Exo and MSC^{TAD}-Exo exhibited a similar protective effect on cardiac function (Figure 7H, K and Supplementary Figure 6C). Regarding the morphological effect of the pulmonary artery, $MSC^{TAD(antagomir)}$-Exo increased vascular remodeling compared with MSC^{TAD}-EXO, whereas $MSC^{(agomir)}$-Exo and MSC^{TAD}-EXO had a similar positive effect on vascular remodeling

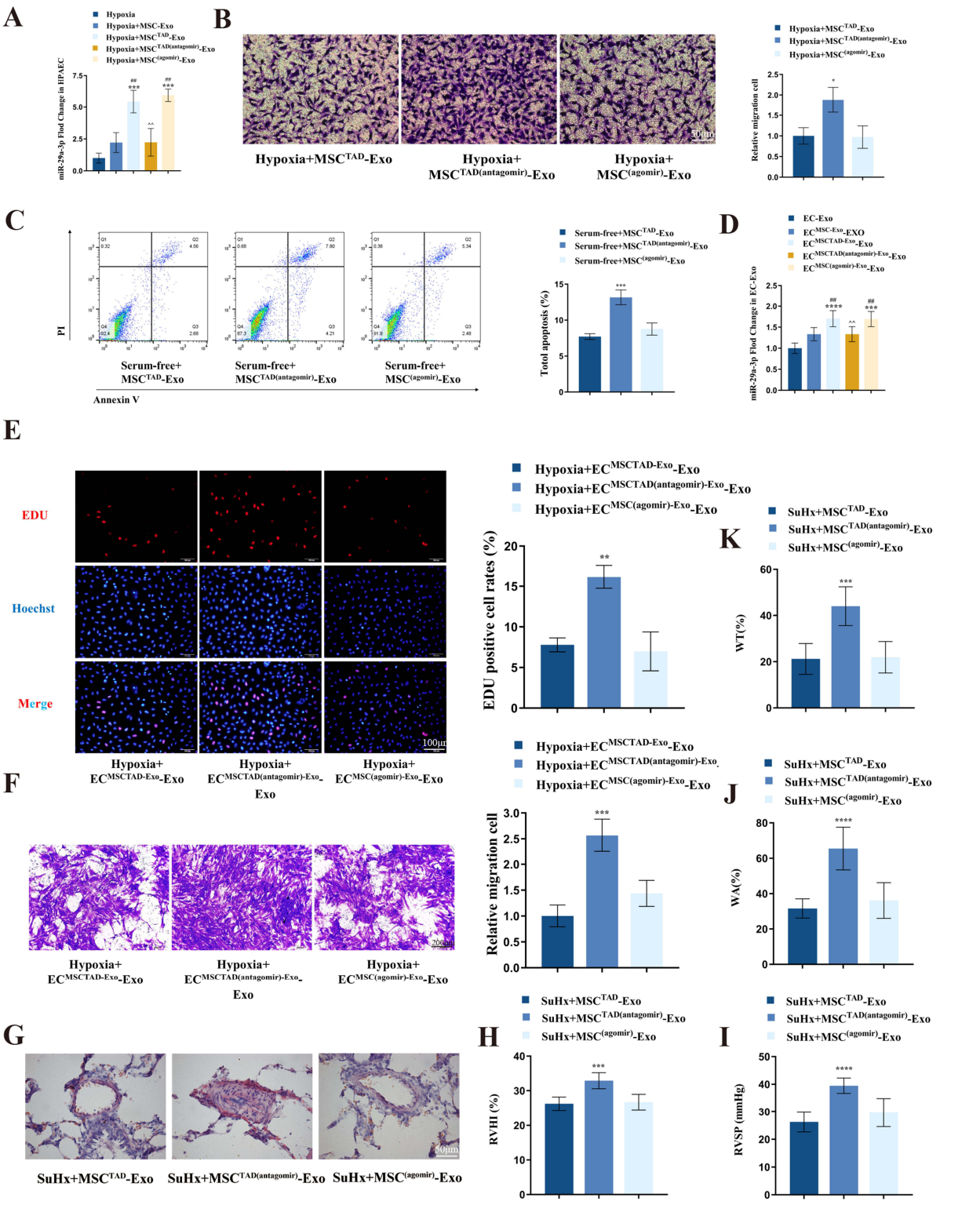

Figure 7 MSC^{TAD}-Exo treats hypoxia-induced pulmonary hypertension by delivering miR-29a-3p. (**A**) The expression values for miR-29a-3p in HPAECs treated by different exosomes. (n = 3) ***P < 0.001 vs Hypoxia; $^{\#\#}P$ < 0.01 vs Hypoxia+ MSC-Exo; $^{\wedge\wedge}P$ < 0.01 vs Hypoxia+ MSC^{TAD}-Exo; (**B**) HPAECs migration was assessed using Transwell assay. (n = 6) *P < 0.05 vs Hypoxia+ MSC^{TAD}-Exo; (**C**) Scatter plot of apoptosis detected by flow cytometry. (n = 3) ***P < 0.001 vs Serum-free+ MSC^{TAD}-Exo; (**D**) The expression values for miR-29a-3p in HPASMCs treated by different exosomes (n = 3). ***P < 0.001, ****P < 0.0001 vs EC-Exo; $^{\#\#}P$ < 0.01 vs EC$^{MSC\text{-}Exo}$-Exo; $^{\wedge\wedge}P$ < 0.01 vs EC$^{MSCTAD\text{-}Exo}$-Exo; (**E**) Cell proliferation was assessed using Edu experiments (n = 3). Scale bar = 100 μm. (**F**) HPASMCs migration was assessed by using Transwell assay. **P < 0.01, ***P < 0.001 vs EC$^{MSCTAD\text{-}Exo}$-Exo; (**G**) Representative image of HE staining performed to quantify the medial wall thickness of distal vessels. Scale bar = 50 μm. (**H**) Calculated as the weight ratio of RV and LV + S (RV/LV + (S). (**I**) RVSP was measured by right-sided heart catheterization with a pressure transducer microcatheter. (**J**) The proportion of the medial wall area. (**K**) The proportion of the medial wall thickness. (**E**–**K**) n = 6. ***P < 0.001, ****P < 0.0001 vs SuHx+ MSC^{TAD}-Exo.

Table 2 Hemodynamic and Morphologic Data

	SuHx + MSC^{TAD}-Exo	SuHx + MSCTAD (antagomir)-Exo	SuHx + MSC (agomir)-Exo
RVSP (mmHg)	26.2±3.6	39.5±2.7****	29.7±5.1
RVHI (%)	26.2±1.8	32.9±2.1***	26.7±2.0
WA (%)	31.4±6.0	65.5±12.1****	35.7±11.2
WT (%)	21.2±6.6	44.0±8.3***	21.9±6.7
Treadmill Distance (m)	306.7±51.5	163.3±33.8***	315±44.3

Notes: ***P < 0.001, ****P < 0.0001 vs SuHx+ MSC^{TAD}-Exo.

(Figure 7G–K and Table 2). Collectively, these results suggest that MSC^{TAD}-Exo improves vascular remodeling and protects the right ventricular function at least in part through miR-29a-3p.

Discussion

In the present study, exosomes derived from bone marrow MSCs and pretreated with TAD for 48 h are a good source of exosomes for PH treatment. TAD pretreatment significantly enhanced the anti-inflammatory capacity of the MSC-Exo, inhibited EC apoptosis in the serum-free medium, decreased hypoxia-induced EC migration, and attenuated the promotional effect of ECs on SMC proliferation and migration under hypoxic conditions. The MSC^{TAD}-Exo reduced pulmonary arterial pressure, improved vascular remodeling, and restored the right ventricular function in the rat hypoxia model. These beneficial effects of exosomes may be mediated through miR-29a-3p. TAD upregulated miR-29a-3p expression in MSCs by facilitating CREB1 binding to the promoter region (at −832 to −839 bp) of miR-29a-3p. MiR-29a-3p can be secreted into Raw264.7 cells through exosomes to exert its potent anti-inflammatory effect by affecting the ENPP2 protein level. Additionally, miR-29a-3p can also be taken up by ECs via exosomes to resist apoptosis and migration, and affected EC-secreted exosomes and further attenuated the pro-proliferative and pro-migratory effects of ECs on SMCs under hypoxic conditions. In vivo, miR-29a-3p in MSC^{TAD}-Exo was a crucial player in attenuating vascular remodeling, lowering right ventricular pressure, and restoring the right ventricular function. In summary, we found that $MSC^{TAD\text{-}Exo}$ enhances three cellular functions during vascular remodeling in pulmonary hypertension by delivering miRNA-29a-3p. Specifically, it: ① Inhibits the expression of ENPP2 in macrophages, exerting a powerful anti-inflammatory effect; ② Inhibits the proliferation, migration and apoptosis of endothelial cells; and ③ Improves the exosomes secreted by endothelial cells, thereby alleviating the proliferation and migration of smooth muscle cells. Notably, the increase in miRNA-29a-3p within $MSC^{TAD\text{-}Exo}$ is attributed to tadalafil's activation of the binding of the CREB1 promoter to the promoter region of miRNA-29a-3p. To our knowledge, this is the first study in which TAD pretreatment of MSCs resulted in the production of better-valued exosomes, which in turn exerted vascular and cardiac protective effects.

Compared with stem cell transplantation, exosome therapy for PH produces similar effects but offers the advantage of being less immunogenic and free of teratoma formation. PH treatment with MSC-Exo has recently been reported. Such exosomes can improve vascular remodeling and the right ventricular function while decreasing the inflammatory reaction.[35–37] Some efforts have been exerted to develop modified stem cell-derived exosomes, which could play a superior role in disease treatment. For example, TNFα-treated MSCs further heightened the neuroprotective effects of exosomes in retinal ischemic injury by increasing miR-21a-5p expression.[18] After Hemin overexpression, MSCs offer better protection against myocardial infarction by increasing miR-283-5p expression.[38] In acute myocardial infarction, atorvastatin increases the therapeutic efficacy of MSC-Exo by upregulating long non-coding RNA H19.[16] However, to our knowledge, modification of MSC-Exo has not been investigated in PH treatment. TAD pretreatment of MSCs is remarkably more clinically feasible, and so, our study may have a direct translational impact on the treatment of PH patients.

In PH, vascular remodeling and inflammatory infiltration are the most prominent pathological changes, with right ventricular failure being the main cause of death in PH patients.[39,40] Vascular remodeling is often characterized by an increase in intima-media thickness and accompanied by infiltration of perivascular inflammatory cells and release of inflammatory factors.[41] MSC-Exo can adequately ameliorate the complete process of vascular remodeling and inflammatory reactions. However, our data

revealed that MSC^{TAD}-Exo has stronger anti-inflammatory and antivascular remodeling capacities and causes an improvement in the right ventricular function compared with exosomes secreted by untreated MSCs (Figures 2 and 3).

In this stage of vascular remodeling, ECs crosstalk with SMCs. Under hypoxia, ECs often promote SMC proliferation and migration by secreting various factors including proteins and exosomes. For example, Zou Xiaozhou et al demonstrated that HPAECs activated SMCs and promoted their proliferation by delivering miR-224-5p-abundant exosomes in PH.[15] According to Lizhong Du et al, PVEC-derived exosomes activated SMC proliferation and migration by carrying miR-214-3p and miR-326-3p.[27] These findings suggest that the crosstalk between ECs and SMCs is critical in the complex vascular remodeling process. Moreover, improving this process may exert an ameliorative effect on vascular remodeling. In this study, on staining MSC-Exo with PHK26, we found for the first time that HPAECs significantly internalized these exosomes, but HPASMCs did not (Figures 1D and 4A). The exact underlying mechanism is unknown, but this may be partly related to the mosaic of connexins and integrins present in the exosome membranes of different cell types. On investigating the effects of MSC-Exo on HPASMCs under hypoxia, we observed that stimulating HPASMCs with MSC^{TAD}-Exo did not alter HPASMC proliferation and migration, whereas stimulating HPASMCs with $EC^{MSC(TAD)\text{-}Exo}$-Exo significantly attenuated cell proliferation and migration (Figure 4). These results suggest that the exosome uptake efficiency of each cell is different. The clinical application of therapeutic exosomes requires a deeper understanding of exosome uptake and its specific mechanisms so as to capitalize on their beneficial effects.

Exosomes containing proteins, mRNAs, and miRNAs can be transferred to cells to regulate their signaling pathways.[42] Increasing evidence has shown that exosomal miRNAs mediate many biological processes, but However, the role of exosomal miRNAs from stem cells is poorly studied in PH. Biogenesis of miR-29a-3p, like that of other miRNAs, begins in the nucleus and then moves to the cytoplasm. A mature miRNA duplex is formed from pri-miRNA and pre-miRNA once they are transcribed by RNA polymerase II and cleaved primarily by the RNase III enzymes Drosha and Dicer.[43] MiR-29a-3p expression is decreased in a PH model, whereas its overexpression improves myocardial function and attenuates hypoxic PH.[31,32] In the present study, miR-29a-3p was more highly expressed in MSC^{TAD}-Exo than in MSC-Exo (Figure 5A). Thus, we proposed that miR-29a-3p is a major active component in MSC^{TAD}-Exo.

Additionally, a further mechanism study revealed that TAD pretreatment of MSCs increases CREB1 protein expression and promotes CERB1 binding in the miR-29a-3p promoter region, thereby leading to further upregulation of miR-29a-3p expression. CREB1 is a basic leucine zipper class transcription factor. It can serve as a homodimer or heterodimer with DNA binding. CREB1 is crucial for responding to various extracellular signals and regulating gene expression.[44] In our study, dual-luciferase reporter gene assay and CHIP-qPCR assay revealed that CREB1 binds at −832 to −839 bp of the miR-29a-3p promoter, and adding TAD to MSCs and CREB1 knockdown significantly reduce miR-29a-3p expression, suggesting the key role played by CREB1 in TAD-promoted miR-29a-3p expression (Figure 5).

On the other hand, miR-29a-3p levels were significantly elevated in both RAW264.7 cells and HPAECs after MSC^{TAD}-Exo treatment. The same results were also observed by adding MSC(agomir)-Exo in the two types of cells. To investigate the anti-inflammatory mechanism of miR29a-3p in macrophages, ENPP2 was predicted as a potential target of miR29a-3p by using TargetScan and the miRBD database. ENPP2 is a well-established protein with lysophospholipase D activity and is significantly overexpressed in various inflammatory diseases.[33,34] When ENPP2 expression in Raw264.7 cells is inhibited, inflammatory responses are significantly reduced.[45,46] MiR-29a-3p exhibited significant anti-inflammatory capacities when MSC(agomir)-Exo was added to the RAW264.7 cells. The overexpression of ENPP2 in the RAW264.7 cells significantly attenuated the anti-inflammatory effect of miR-29a-3p. Furthermore, through the dual luciferase reporter gene assay, we verified that miR-29a-3p binds to ENPP2 at the 3′UTR (Figure 6). Based on the aforementioned data, we illustrated that miR-29a-3p exerts its anti-inflammatory effects through ENPP2. When miR-29a-3p expression was silenced in the TAD-pretreated MSCs, the antiapoptotic and antimigration effects of MSC^{TAD}-Exo on ECs were attenuated, and the ECs regained their pro-proliferative and pro-migration effect on SMCs. In vivo, the same results were detected that the therapeutic effects of MSC^{TAD}-Exo were significantly attenuated with miR-29a-3p knockdown in MSC^{TAD}-Exo. MSC^{TAD}-Exo exhibiting miR-29a-3p overexpression had the same therapeutic effects on SuHx-induced PH rats (Figure 7). These results support that miR-29a-3p is a potent therapeutic component in MSC^{TAD}-Exo.

A successful treatment for PH may involve a combination of beneficial effects that counteract vascular remodeling and inflammation and improve the right ventricular function. Although MSC^{TAD}-Exo exhibited significantly improved

therapeutic efficacy compared with MSC-Exo, further clinical studies are warranted to validate the efficacy and safety of this strategy before it becomes a therapeutic approach for PH. On the other hand, whether this approach for improving vascular remodeling can be applied to other vascular diseases needs to be explored. In conclusion, our study has set a precedent in the pulmonary arterial hypertension field by utilizing drug-modified stem cells to treat this condition and provides a new feasible option for PH treatment.

Conclusion

We found that MSC^{TAD}-Exo had better efficacy than MSC-Exo in the treatment of pulmonary hypertension, and further revealed the mechanism of action by which MSC^{TAD}-Exo exerts its function.

Highlights

- We found for the first time that exosomes secreted by mesenchymal stem cells after tadalafil addition have better efficacy in the treatment of pulmonary arterial hypertension
- This study reveals the transcriptional regulation between CREB1 and miR-29a-3p
- This study identifies an anti-inflammatory effect of miR-29a-3p through enpp2
- The article reveals for the first time that in vivo smooth muscle cells take up exosomes via endothelial cells

Abbreviations

PH, Pulmonary hypertension; Exo, Exosomes; TAD, Tadalafil; MSC, Mesenchymal stem cell; HPAEC, Human pulmonary artery endothelial cell; CREB1, cAMP responsive element binding protein 1; ENPP2, Ectonucleotide pyrophosphatase/phosphodiesterase 2; HPASMC, Human pulmonary artery smooth muscle cell; RVSP, Right ventricular systolic pressure; LV, Left ventricle; RVHI, RV hypertrophy; WT, wall thickness; WA, wall area.

Data Sharing Statement

The original data are included in the article and supplementary materials. Further inquiries can be directed to the corresponding authors. The authors will offer the raw data supporting the conclusions of this article without undue reservation.

Ethics Approval and Consent to Participate

The Jinzhou Medical University Research Ethics Committee approved all animal testing and procedures (2022031001).

Consent for Publication

All authors of this study agreed to publish.

Author Contributions

Yi Liu: Writing of the original draft, methodology, and visualization. Changqing He and Quanhai Zhong: Methodology. Xianbao Shi: Funding acquisition. Hongyan Li and Gaoge Fu: Validation and methodology. Lixuan Guo and Churong Zhao: Investigation. Lei Tian: Investigation. Xin Li and Xue Jiao: Funding acquisition. Lina Shan: Conceptualization, writing, review, and editing of the manuscript, project administration, and funding acquisition. All authors made a significant contribution to the work reported, whether that is in the conception, study design, execution, acquisition of data, analysis and interpretation, or in all these areas; took part in drafting, revising or critically reviewing the article; gave final approval of the version to be published; have agreed on the journal to which the article has been submitted; and agree to be accountable for all aspects of the work.

Funding

The study was financially sponsored the funding of Scientific Research of The First Affiliated Hospital of Jinzhou Medical University (KYTD-2022003) and Liaoning Revitalization Talents Program (XLY2007142).

Disclosure

No potential conflict of interest needs to be stated.

References

1. Galie N, Channick RN, Frantz RP, et al. Risk stratification and medical therapy of pulmonary arterial hypertension. *Eur Respir J*. 2019;53:1801889. doi:10.1183/13993003.01889-2018
2. Heath D, Edwards JE. The pathology of hypertensive pulmonary vascular disease; a description of six grades of structural changes in the pulmonary arteries with special reference to congenital cardiac septal defects. *Circulation*. 1958;18:533–547. doi:10.1161/01.CIR.18.4.533
3. Baber SR, Deng W, Master RG, et al. Intratracheal mesenchymal stem cell administration attenuates monocrotaline-induced pulmonary hypertension and endothelial dysfunction. *Am J Physiol Heart Circ Physiol*. 2007;292:H1120–1128. doi:10.1152/ajpheart.00173.2006
4. Kanki-Horimoto S, Horimoto H, Mieno S, et al. Implantation of mesenchymal stem cells overexpressing endothelial nitric oxide synthase improves right ventricular impairments caused by pulmonary hypertension. *Circulation*. 2006;114:I181–185. doi:10.1161/CIRCULATIONAHA.105.001487
5. Huang WC, Ke MW, Cheng CC, et al. Therapeutic Benefits of Induced Pluripotent Stem Cells in Monocrotaline-Induced Pulmonary Arterial Hypertension. *PLoS One*. 2016;11:e0142476. doi:10.1371/journal.pone.0142476
6. Yang JX, Pan YY, Zhao YY, Wang XX. Endothelial progenitor cell-based therapy for pulmonary arterial hypertension. *Cell Transplant*. 2013;22:1325–1336. doi:10.3727/096368912X659899
7. Umar S, de Visser YP, Steendijk P, et al. Allogenic stem cell therapy improves right ventricular function by improving lung pathology in rats with pulmonary hypertension. *Am J Physiol Heart Circ Physiol*. 2009;297:H1606–1616. doi:10.1152/ajpheart.00590.2009
8. Makridakis M, Roubelakis MG, Vlahou A. Stem cells: insights into the secretome. *Biochim Biophys Acta*. 2013;1834:2380–2384. doi:10.1016/j.bbapap.2013.01.032
9. Gnecchi M, Zhang Z, Ni A, Dzau VJ. Paracrine mechanisms in adult stem cell signaling and therapy. *Circ Res*. 2008;103:1204–1219. doi:10.1161/CIRCRESAHA.108.176826
10. Zhang Z, Ge L, Zhang S, et al. The protective effects of MSC-EXO against pulmonary hypertension through regulating Wnt5a/BMP signalling pathway. *J Cell Mol Med*. 2020;24:13938–13948.
11. Zhang S, Wang J, Wen J, et al. MSC-derived exosomes attenuates pulmonary hypertension via inhibiting pulmonary vascular remodeling. *Exp Cell Res*. 2024;442:114256. doi:10.1016/j.yexcr.2024.114256
12. Han QF, Li WJ, Hu KS, et al. Exosome biogenesis: machinery, regulation, and therapeutic implications in cancer. *Mol Cancer*. 2022;21:207. doi:10.1186/s12943-022-01671-0
13. Deng L, Blanco FJ, Stevens H, et al. MicroRNA-143 Activation Regulates Smooth Muscle and Endothelial Cell Crosstalk in Pulmonary Arterial Hypertension. *Circ Res*. 2015;117:870–883. doi:10.1161/CIRCRESAHA.115.306806
14. Yuan K, Shamskhou EA, Orcholski ME, et al. Loss of Endothelium-Derived Wnt5a Is Associated With Reduced Pericyte Recruitment and Small Vessel Loss in Pulmonary Arterial Hypertension. *Circulation*. 2019;139:1710–1724. doi:10.1161/CIRCULATIONAHA.118.037642
15. Zou X, Liu T, Huang Z, et al. SOX17 is a Critical Factor in Maintaining Endothelial Function in Pulmonary Hypertension by an Exosome-Mediated Autocrine Manner. *Adv Sci*. 2023;10:e2206139. doi:10.1002/advs.202206139
16. Huang P, Wang L, Li Q, et al. Atorvastatin enhances the therapeutic efficacy of mesenchymal stem cells-derived exosomes in acute myocardial infarction via up-regulating long non-coding RNA H19. *Cardiovasc Res*. 2020;116:353–367. doi:10.1093/cvr/cvz139
17. Feng W, Jin Q, Ming-Yu Y, et al. MiR-6924-5p-rich exosomes derived from genetically modified Scleraxis-overexpressing PDGFRalpha(+) BMMSCs as novel nanotherapeutics for treating osteolysis during tendon-bone healing and improving healing strength. *Biomaterials*. 2021;279:121242. doi:10.1016/j.biomaterials.2021.121242
18. Yu Z, Wen Y, Jiang N, et al. TNF-alpha stimulation enhances the neuroprotective effects of gingival MSCs derived exosomes in retinal ischemia-reperfusion injury via the MEG3/miR-21a-5p axis. *Biomaterials*. 2022;284:121484. doi:10.1016/j.biomaterials.2022.121484
19. Haider H, Lee YJ, Jiang S, Ahmed RP, Ryon M, Ashraf M. Phosphodiesterase inhibition with tadalafil provides longer and sustained protection of stem cells. *Am J Physiol Heart Circ Physiol*. 2010;299:H1395–1404. doi:10.1152/ajpheart.00437.2010
20. Kumar S, Ashraf M. Tadalafil, a Phosphodiesterase Inhibitor Protects Stem Cells over Longer Period Against Hypoxia/Reoxygenation Injury Through STAT3/PKG-I Signaling. *Stem Cells Dev*. 2015;24:1332–1341. doi:10.1089/scd.2014.0288
21. Fischer UM, Harting MT, Jimenez F, et al. Pulmonary passage is a major obstacle for intravenous stem cell delivery: the pulmonary first-pass effect. *Stem Cells Dev*. 2009;18:683–692. doi:10.1089/scd.2008.0253
22. Eggenhofer E, Luk F, Dahlke MH, Hoogduijn MJ. The life and fate of mesenchymal stem cells. *Front Immunol*. 2014;5:148. doi:10.3389/fimmu.2014.00148
23. Abe K, Toba M, Alzoubi A, et al. Formation of Plexiform Lesions in Experimental Severe Pulmonary Arterial Hypertension. *Circulation*. 2010;121:2747–2754. doi:10.1161/CIRCULATIONAHA.109.927681
24. Liu M, Tao G, Cao Y, Hu Y, Zhang Z. Silencing of IGF2BP1 restrains ox-LDL-induced lipid accumulation and inflammation by reducing RUNX1 expression and promoting autophagy in macrophages. *J Biochem Mol Toxicol*. 2022;36:e22994. doi:10.1002/jbt.22994
25. Han M, Yang H, Lu X, et al. Three-Dimensional-Cultured MSC-Derived Exosome-Hydrogel Hybrid Microneedle Array Patch for Spinal Cord Repair. *Nano Lett*. 2022;22:6391–6401. doi:10.1021/acs.nanolett.2c02259
26. Zhou T, He C, Lai P, et al. miR-204-containing exosomes ameliorate GVHD-associated dry eye disease. *Sci Adv*. 2022;8:eabj9617. doi:10.1126/sciadv.abj9617
27. Luo X, Hang C, Zhang Z, et al. PVECs-Derived Exosomal microRNAs Regulate PASMCs via FoxM1 Signaling in IUGR-induced Pulmonary Hypertension. *J Am Heart Assoc*. 2022;11:e027177. doi:10.1161/JAHA.122.027177
28. Zheng D, Huo M, Li B, et al. The Role of Exosomes and Exosomal MicroRNA in Cardiovascular Disease. *Front Cell Dev Biol*. 2020;8:616161. doi:10.3389/fcell.2020.616161
29. Isaac R, Reis FCG, Ying W, Olefsky JM. Exosomes as mediators of intercellular crosstalk in metabolism. *Cell Metab*. 2021;33:1744–1762. doi:10.1016/j.cmet.2021.08.006

30. Chen T, Sun MR, Zhou Q, et al. Extracellular vesicles derived from endothelial cells in hypoxia contribute to pulmonary artery smooth muscle cell proliferation in-vitro and pulmonary hypertension in mice. *Pulm Circ*. 2022;12:e12014. doi:10.1002/pul2.12014
31. Hsu CH, Liu IF, Kuo HF, et al. miR-29a-3p/THBS2 Axis Regulates PAH-Induced Cardiac Fibrosis. *Int J Mol Sci*. 2021;22:10574. doi:10.3390/ijms221910574
32. Luo Y, Dong HY, Zhang B, et al. miR-29a-3p attenuates hypoxic pulmonary hypertension by inhibiting pulmonary adventitial fibroblast activation. *Hypertension*. 2015;65:414–420. doi:10.1161/HYPERTENSIONAHA.114.04600
33. Linden J, Koch-Nolte F, Dahl G. Purine Release, Metabolism, and Signaling in the Inflammatory Response. *Annu Rev Immunol*. 2019;37:325–347. doi:10.1146/annurev-immunol-051116-052406
34. Plastira I, Bernhart E, Joshi L, et al. MAPK signaling determines lysophosphatidic acid (LPA)-induced inflammation in microglia. *J Neuroinfl*. 2020;17:127. doi:10.1186/s12974-020-01809-1
35. Aliotta JM, Pereira M, Wen S, et al. Exosomes induce and reverse monocrotaline-induced pulmonary hypertension in mice. *Cardiovasc Res*. 2016;110:319–330. doi:10.1093/cvr/cvw054
36. Lee C, Mitsialis SA, Aslam M, et al. Exosomes mediate the cytoprotective action of mesenchymal stromal cells on hypoxia-induced pulmonary hypertension. *Circulation*. 2012;126:2601–2611. doi:10.1161/CIRCULATIONAHA.112.114173
37. Zhang S, Liu X, Ge LL, et al. Mesenchymal stromal cell-derived exosomes improve pulmonary hypertension through inhibition of pulmonary vascular remodeling. *Respir Res*. 2020;21:71. doi:10.1186/s12931-020-1331-4
38. Zheng H, Liang X, Han Q, et al. Hemin enhances the cardioprotective effects of mesenchymal stem cell-derived exosomes against infarction via amelioration of cardiomyocyte senescence. *J Nanobiotechnol*. 2021;19:332. doi:10.1186/s12951-021-01077-y
39. Nathan SD, Barbera JA, Gaine SP, et al. Pulmonary hypertension in chronic lung disease and hypoxia. *Eur Respir J*. 2019;53:1801914. doi:10.1183/13993003.01914-2018
40. Thompson AAR, Lawrie A. Targeting Vascular Remodeling to Treat Pulmonary Arterial Hypertension. *Trends Mol Med*. 2017;23:31–45. doi:10.1016/j.molmed.2016.11.005
41. Naeije R, Richter MJ, Rubin LJ. The physiological basis of pulmonary arterial hypertension. *Eur Respir J*. 2022;59:2102334. doi:10.1183/13993003.02334-2021
42. Noonin C, Thongboonkerd V. Exosome-inflammasome crosstalk and their roles in inflammatory responses. *Theranostics*. 2021;11:4436–4451. doi:10.7150/thno.54004
43. Mo WY, Cao SQ. MiR-29a-3p: a potential biomarker and therapeutic target in colorectal cancer. *Clin Transl Oncol*. 2023;25:563–577. doi:10.1007/s12094-022-02978-6
44. Martin LJ, Nguyen HT. Basic Leucine Zipper Transcription Factors as Important Regulators of Leydig Cells' Functions. *Int J Mol Sci*. 2022;23:12887. doi:10.3390/ijms232112887
45. Wang Z, Shi W, Tian D, et al. Autotaxin stimulates LPA2 receptor in macrophages and exacerbates dextran sulfate sodium-induced acute colitis. *J Mol Med*. 2020;98:1781–1794. doi:10.1007/s00109-020-01997-6
46. Jing T, Miao X, Jiang F, et al. Discovery and optimization of tetrahydropyrido[4,3-d]pyrimidine derivatives as novel ATX and EGFR dual inhibitors. *Bioorg Med Chem*. 2018;26:1784–1796. doi:10.1016/j.bmc.2018.02.023